Archimedean Screw Turbine Based Energy Harvester and Acoustic Communication in Well Site Applications

Rui Lin

Thesis submitted to the Faculty of the
Virginia Polytechnic Institute and State University
in partial fulfillment of the requirements for the degree of

Master of Science
in
Mechanical Engineering

Lei Zuo, Chair
Tomonari Furukawa
Muhammad R. Hajj
Robert G. Parker

November 19, 2019
Blacksburg, Virginia

Keywords: Energy Harvesting, Archimedean Screw Turbine, Acoustic Communication, Oil and Gas Industry

Archimedean Screw Turbine Based Energy Harvester and Acoustic Communication in Well Site Applications

Rui Lin

ABSTRACT

Wireless Sensor Networks (WSNs) has become increasingly important in the Oil and Gas industry. Despite the various advantages WSN has compared to the wired counter parts, it also faces some critical challenges in the oil fields; one of them is the power supply. The periodic replacement of batteries for the WSN in the downhole environments has been economically inconvenient and the enormous cost induced by the maintenance has turned people's attention to the energy harvesting technology, hoping for a more sustainable solution. Power supply is only half of the problem. To retrieve the data recorded by the various sensors in the downhole environments, a reliable way of wireless communication is required. A new approach utilizing acoustic communication was proposed. This thesis presents an Archimedean Screw Turbine (AST) based energy harvester that takes advantage of the abundant flow energy in the upper stream section of the oil production cycle, especially in the water injection wells and oil extraction wells, with the goal of providing power supply to Wireless Sensor Networks (WSNs) and underwater acoustic modems deployed in the various locations in the downhole environments. Parametric study on the number of blades, screw length, screw pitch, and rotational speed was conducted through CFD analysis using $AnsysFluent$ in order to determine the optimal geometry and operating conditions. The relationship between power generation and AST geometries, such as AST length and AST pitch, were discovered and the optimal rotational speed was revealed to be solely dependent on the screw pitch. Experiments were conducted in the lab environment with various flow rates and various external resistive loads to verify and determine the maximum power generation of the designed harvester. FEA analysis was conducted using the $AcousticandStructuralInteractionModule$ of $COMSOLMULTIPHYSICS$ to determine the attenuation characteristics of acoustic waves propagating in the water-filled pipes buried in soil. Experiments with and without the harvester integrated in the pipe system were conducted in lab environment using a pair of under water acoustic modems to determine the acoustic communication capability. The impact of the integrated harvester on the acoustic communication was tested. Combining energy harvesting technology and underwater acoustic communication together, this system can potentially achieve real-time monitoring and communication in the oil downhole environment.

The author would like to thank the partial financial support from NSF Grant #CMMI-1529842 and DOE Grant #DE-NE0008591 during the study.

Archimedean Screw Turbine Based Energy Harvester and Acoustic Communication in Well Site Applications

Rui Lin

GENERAL AUDIENCE ABSTRACT

Oil and Gas industry has been the primary energy source provider for our society for hundreds of years. As this industry evolves with new technologies, it also faces new challenges. One of the main challenges is the power supply problem in the oil field because of the limited lifespan of traditional batteries used in the oil production process. This study present a novel energy harvesting device that can replace the traditional batteries. By taking advantage of the constant fluid flow in various wells at oil field, the device can provide power for electronic devices, including but not limited to wireless sensors, communication modules, at the oil extraction sites, without needing additional power supply. This novel energy harvesting device can also be integrated with communication modules that uses acoustic wave to achieve wireless acoustic communication between underground and the surface. In this study, the harvester design, optimization, tests, and integration with acoustic modems were presented. With the help of such energy harvesting device, Oil and Gas industry will be one step closer to achieving true wireless, and real-time monitoring and communication. This will not only reduce maintenance cost but also greatly improve the production efficiency.

Contents

List of Figures

List of Tables

Chapter 1

Introduction

1.1 Wireless Sensing in Oil and Gas Industry

Smart technologies and infrastructures are playing an increasingly critical role in many fields including oil and gas industry. Wireless sensor networks and communication systems are attracting growing attention due to the inherent benefits compared to the traditional, wired systems. Without the constrain of the wires, wireless sensor nodes are more flexible in terms of installation. This often allows the sensors to be placed much closer to the locations where the measurement of interest is. Therefore, wireless sensor networks can provide increased measurement accuracy and density compared to the traditional, wired counterpart (Gungor et al., 2009). With high speed communication and advanced processors, data from hundreds or thousands of sensing nodes can be transmitted, processed, and stored in real time (Huo et al., 2010).

Wireless sensing and controls are implemented throughout the oil production cycles, including drilling, water injection, extraction, refinery, pipeline and transportation. Sensors are adopted in these processes to provide production parameters such as temperature, pressure, and flow rate to maximize the production efficiency or reduce equipment wear.

Due to the advancement of the microelectromechanical system (MEMS), and the reduction of wireless sensor cost, there has been a paradigm shift from the traditional wired system to the wireless system. According to a report by Research and Market, the global wireless sensor networks (WSN) revenues for oil and gas industry will reach 2.2 billion dollars in 2030, up from 480 million dollars in 2017. This is especially beneficial to the oil and gas industry due to the following reasons (Akhondi et al., 2010).

- The numerous remote and hazardous locations
- The difficulty and cost of introducing new wired devices near pipelines

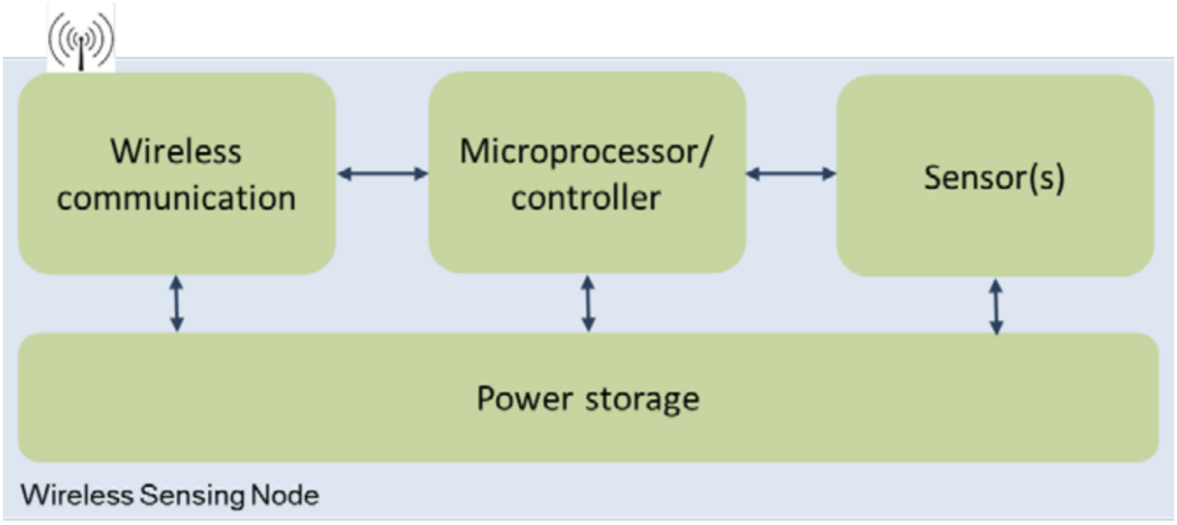

Figure 1.1: WIRELESS SENSING/CONTROL NODE (Ahmad et al., 2013).

- The requirement for temporary sensor installation
- The requirement for sensor redundancy
- The evolution of new control solutions that require further sensors
- The demand for continuous production optimization and growth
- The demand for improved safety

One major challenge to implement WSN in gas and oil industry lies in the power supply (Ahmad et al., 2013). The conventional method of providing operating power to such systems rely solely on batteries. Two major challenges are faced when using this approach. First, despite the advancement of modern battery technology and low power consumption sensors, the battery life time is still limited. Recharging or replacement is required on a timely basis; a fully charged battery usually last three to six months in the downhole environment depending on how frequent the WSN collects and transmits data.

Second, replacing batteries in oil production fields could often requires the shutdown of oil wells and plant operations. Typical oil fields are equipped with hundreds, if not thousands, of wireless sensors. Replacing batteries for every single one of them could be extremely time-consuming and economically inconvenient. Frequent battery replacement could be impractical in certain scenarios when sensor nods are installed deep underground or in hazardous environments. Another popular way is cable wiring, providing power from ground. Although this approach is permanent and does not require recharging on a timely basis, this induces a high initial installation cost. Running electric cables miles through high temperature

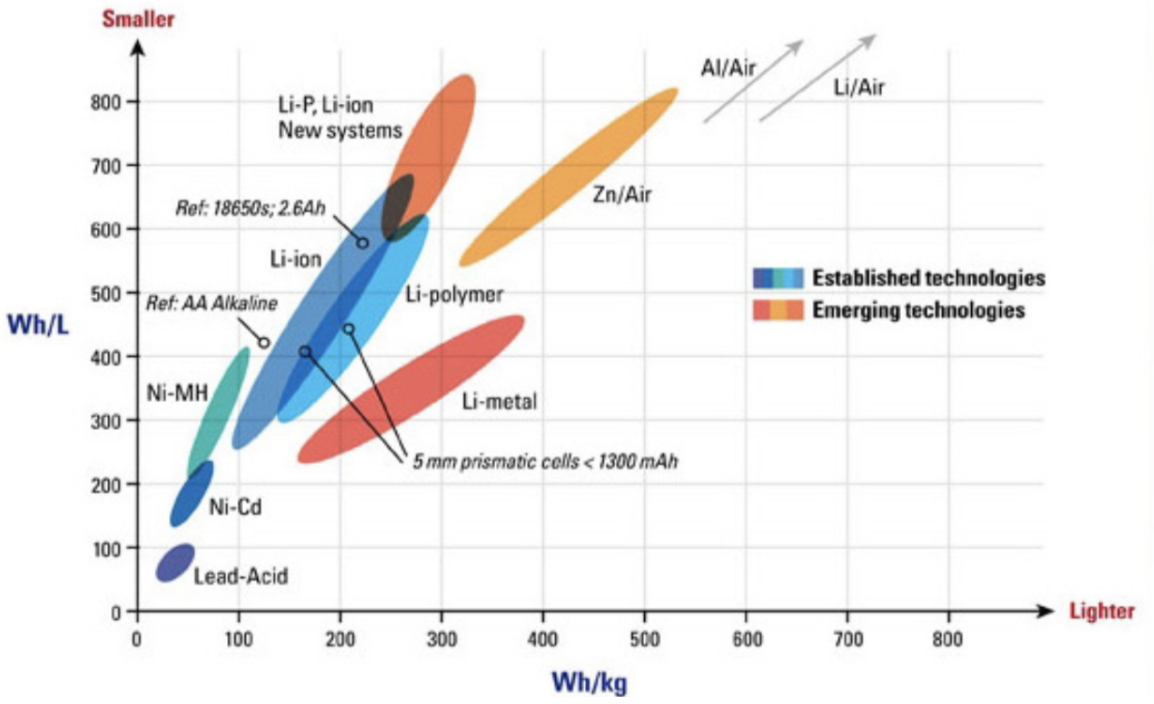

Figure 1.2: ENERGY DENSITY FOR VARIOUS BATTERY CHEMICALS (Ahmad et al., 2013).

and high pressure environment could cause potential electric fire hazard, which is the least thing that people want to have on an oil production field. To address this challenge, people have turned their attention to energy harvesting technology and have been considering it as an emerging solution to the power supply problem of wireless sensors and communication system.

There are several energy sources available for energy harvesting throughout the oil production cycle, including fluid flow, thermal sources, light source, radio frequency, and mechanical energy such as vibration and strain. These wasted/unused energy sources provide the opportunities to build an autonomous WSN and communication system in the oil and gas industry with the help of energy harvesting technology.

1.2 Archimedean Screw Turbine

Among all the energy sources mentioned in the previous section, fluid flow is probably the most prominent one due to its abundant presence throughout the entire production cycle, from production wells to refinery plants and the pipelines connecting between these points. There are multiple ways to extract energy from fluid flow. Aside from flow induced vibration, turbines are the most traditional method when it comes to flow powered device. There are

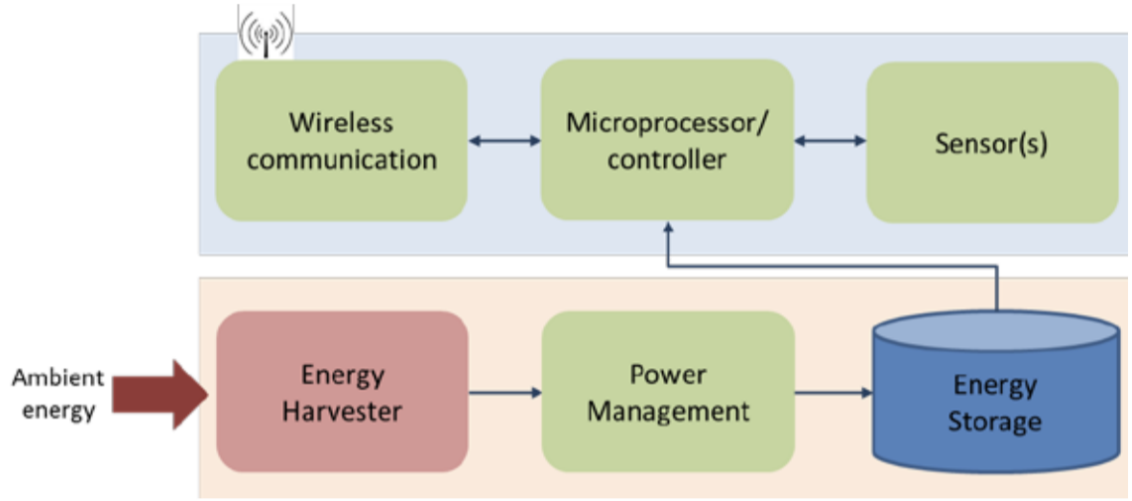

Figure 1.3: ENERGY HARVESTING POWERED WIRELESS SENSING/CONTROL NODE (Ahmad et al., 2013).

several types of turbines that are used to extract hydro powers, the most common ones are Francis turbines and Kaplan turbines. These different types of turbines are suitable for different flow conditions.

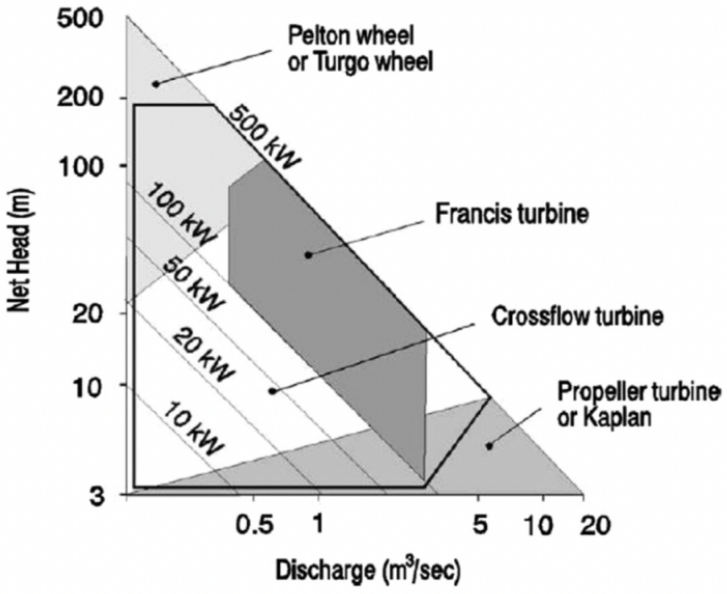

Figure 1.4: HEAD-FLOW RAGES OF SMALL HYDRO TURBINES (Okot et al., 2013).

the Among all types turbines, there is one with unique design, Archimedean Screw Turbine.

An Archimedean Screw Turbine consists of a center cylindrical rod surrounded with several helical spirals running through the length of the rod, which gives it a similar look as a screw. The key geometric parameters an Archimedean screw has are the screw length L, the inner diameter d, which is the diameter of the center cylindrical rod, the outer diameter D, which is the length across the edges of the helical spirals, and the screw pitch P.

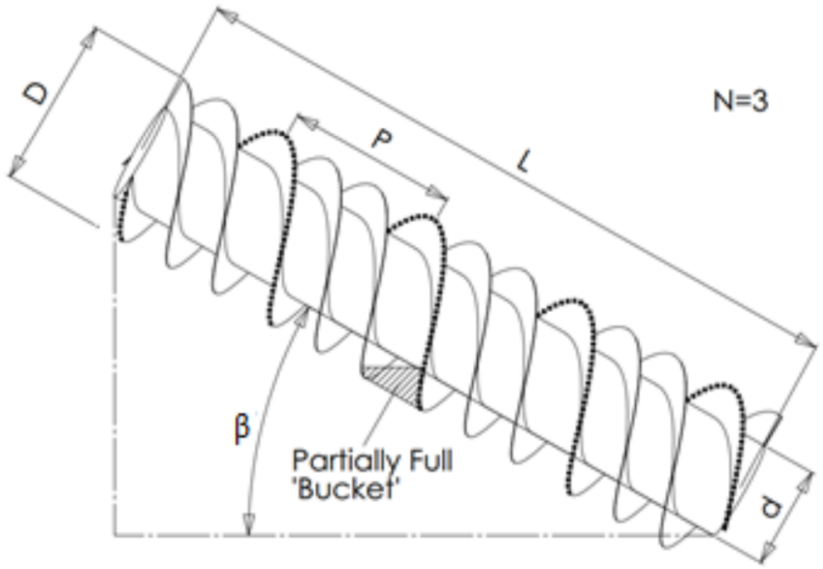

Figure 1.5: BASIC GEOMETRY OF AN AST (Anderson, 2011).

Archimedean screws are one of the oldest inventions of mankind. The origin of this device is still debatable, but it was first designed as a pump to lift and transport heavy weights. Near the end of the 20th century, researchers have reversed its functionality and used it as a low-head turbine to generate electricity. The first applications of Archimedean Screw Generator (ASG) appeared in Europe in the year of 1994 and in UK in the year of 2004 (Waters et al., 2015). Most of the Archimedean Screw Generators (ASGs) are installed over-river due to its unique properties of being fish friendly and requiring low head to operate. ASTs can maintain a high efficiency even as the head approaches zero (Williamson et al., 2015). One study in 2007 showed that ASTs can allow a wide of fish species to pass through with no sustained damage (Kibel et al., 20017). ASTs' extraordinary ability of handling obstacles and debris makes it a much better candidate compared to conventional turbines for oil field related applications where sand and small debris are common in the flow.

1.3 Acoustic Communication

Power supply is only half of the challenge when creating truly wireless sensor networks in oil and gas industry, especially for the downhole applications. Current practice is to use batteries to power said sensors. While replacing the batteries with energy harvesting technology does, in a way, make the system wireless and potentially autonomous, there is still one problem that need to be solved.

On the well sites, pressure sensors and temperature sensors are installed alongside the walls of the oil production wells and water injection wells to measure the conditions of the downhole environment. Currently the data the sensors collected are stored locally and are only accessible when the sensors are taken out for measurement reading. This is because of the unique nature of well site sensing where majority of the sensors are installed thousands of meters underground. The traditional communication methods using electromagnetic wave does not work in this situation because the depth of the soil prevents the electromagnetic wave to penetrate through. to retrieve the data, the sensors need to be taken out of the install locations at a timely basis; this imposes two problems. First, because the install locations are usually deep underground, doing so will impose a tremendously economically inconvenient. It will also requires the occasional pauses during production sessions. Second, these informations collected by sensors are needed to regulate oil production and reduce the equipment wear to achieve maximum efficiency. Since the data collected are only accessible every once in a while, the real-time condition of the downhole environment will never be known; decisions have to be made based on prediction of trends rather than facts.

To make the sensor networks truly wireless, the data collected need to be transmitted and received wirelessly in real time. A reliable way of communication is needed. For the downhole environment, the only pathways connecting the the deep underground and the earth's surface are the wells. This including oil extraction wells, which is used to pump oil to the surface, and water injection wells, which is used to pump water into the underground. Both of these two wells have one thing in common; there are fluid constantly flowing through the well pipes. While it is impossible for electromagnetic wave to propagate through such distance in liquid, it might be a job that pressure waves, such as acoustic waves, can accomplish.

Acoustic waves have long been used for underwater studies. The ability to propagate long distance in media, such as water, enables it for a broad range of applications (Akyildiz et al., 2005). People have envisioned the underwater sensor networks to play an important role in ocean sampling networks (MIT and Florida Atlantic University), environmental monitoring (Yang et al., 2002, Zhang et al., 2004), undersea explorations, disaster prevention (Soreide et al., 2004), assisted navigation, and distributed tactical surveillance (Cayirci et al., 2004). A more comprehensive review of the current of underwater acoustic sensor networks can be found in the work done by Akyildiz et al. in 2005.

The versatility of acoustic wave communication in aquatic environment implies the possibility that the same technology can be used inside wells and pipes that convey various liquid in

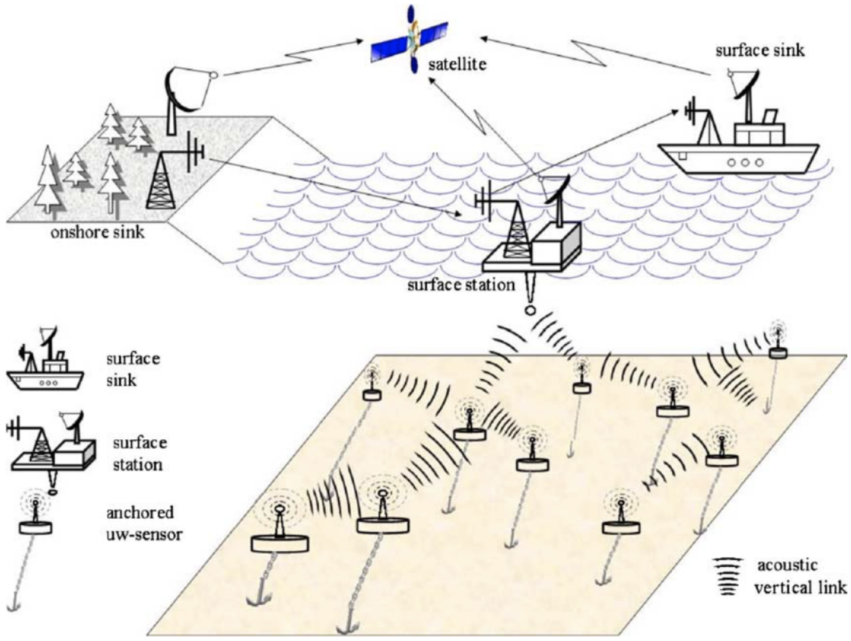

Figure 1.6: ARCHITECTURE OF 3D UNDERWATER SENSOR NETWORKS (Akyildiz et al., 2005).

the oil and gas industry. Combined with energy harvesting technology, a truly wireless, real-time, sensor network that does not require periodic maintenance could be achieved.

1.4 Motivation and Objective

There are increasing demands for wireless sensor networks and communication systems in the modern oil and gas industry. With the limitation of the current battery technology, energy harvesting provides a feasible alternative to the power supply challenge in oil and gas industry, especially on the well site applications. Fluid flow is one of the most common energy source in the oil and gas industry. It is ever present in every single link of oil production process. Flow energy can be seen in water injection, oil extraction, refinery, and miles of pipelines transporting the product through various sites. A device that utilizes this abundant flow energy during the oil production cycle appears to be a promising means for energy harvesting purpose.

Although people have done extensive works on harvesting energy from fluid flow through the means of turbines, the extreme conditions (mainly sand and rock debris mixed in the flow) in the downhole environment make traditional turbines (Kaplan, Francis, Propeller) unsuitable for such application. Compared to the traditional turbines, Archimedean Screw

turbine have several innate advantages. It requires a smaller head for operation, it imposes a less cost for manufacturing and maintenance, and it allows objects in the flow to pass by safely. The various advantages of Archimedean Screw turbine, especially its property to allow obstacles to pass through, make it a much more feasible candidate to harvesting fluid flow energy in the downhole environment.

Currently there are not many literatures on the topic of Archimedean Screw turbines and Archimedean Screw generators. Most of the works on micro hydro power utilizing Archimedean Screw turbines are on the scale of hundreds or thousands of Watts, or even MW; the geometry of the studied systems are too large for in pipe applications in well sites. There are currently no literatures or real world applications of centimeter-scale Archimedean screw for in-pipe applications. Also, the design guidelines for Archimedean Screws are primary intended for pump applications, there are no specific design guidelines for Archimedean Screws as turbines. There are several papers on the theoretical modeling of Archimedean Screw Turbines. However, each of the models have their own limitations.

This research study consists of two parts. First part is to design an Archimedean screw turbine based energy harvester to extract energy from fluid flow in pipes and wells to power sensor networks and communication system in oil and gas industry. The design of the harvester, CFD simulation and optimization, and lab testing are explained in details in the following chapter. The second part of this research study is to investigate the impact of the designed Archimedean Screw Turbine based harvester on the acoustic communication inside water filled pipes/wells. FEA simulations of acoustic wave propagation in water injection well were carried out in an attempt to investigate the attenuation characteristics of acoustic waves. Lab tests were conducted using a pair of acoustic modems from Desert Start to study the impact of the actual harvest on the acoustic communication capability.

Chapter 2

Background and Literature Review

2.1 Energy Harvesting in Oil and Gas Industry

As stated in the previous section, there are several energy sources that are available for energy harvesting in the oil and gas industry. The most common and promising ones are thermal energy, fluid energy, electromagnetic radiation, and mechanical energy such as induced vibration and strains. This section goes through the existing strategies and researches people have done in the past.

2.1.1 Thermal Energy

The most common way to harvest thermal energy is through the thermoelectric energy generators (TEGs), which function based on the principle of Seebeck Effect. When there is temperature difference between two dissimilar electrical conductors or semiconductors, there will be a voltage difference across the two materials (Park et al., 2008). The induced voltage is proportional to the temperature difference (Mateu et al., 2005). Researchers have worked on harvesting thermal energy from automobile exhaust (Vazquez et al., 2002), geothermal (Lawreence et al., 2002), and even human body for medical applications (Hoang et al., 2009). Although there are already a wide range of researches on this phenomenon, and there are commercially available thermalelectric energy harvesting products such as PowerPulse and HoneyWell that can be used on machinery and pipelines, people have yet to apply this technology in the oil and gas industry especially in the downhole environment.

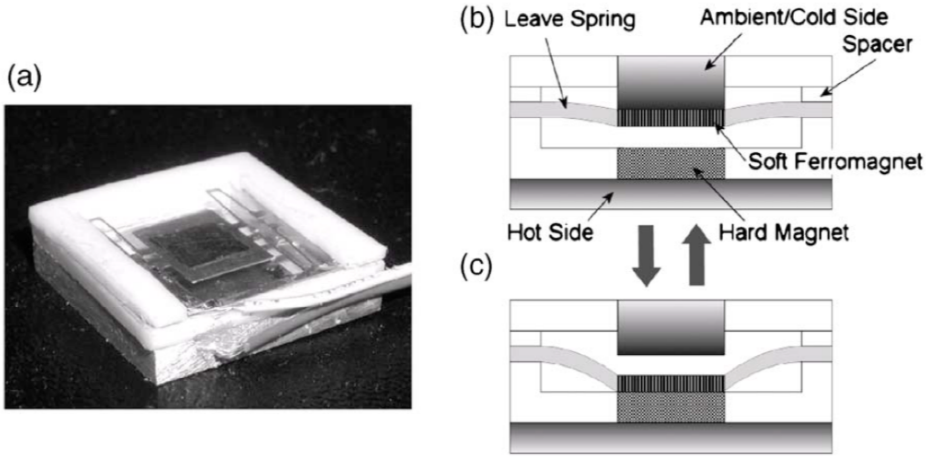

Figure 2.1: THERMALELECTRIC ENERGY HARVESTOR (Ujihara et al., 2013).

2.1.2 Mechanical Energy

Energy harvesting from mechanical sources is one of the most common practices. Mechanical vibration is present through the entire oil production cycle, whether it's vibration from machinery operation or vibration induced by fluid flow in pipelines and oil wells. There are two main mechanisms that are used in energy conversion, electromagnetic and piezoelectric.

Electromagnetic energy harvesting utilize the Farady's law where a changing magnetic field can induce voltage and current flow in nearby conductors (Chalasani et al., 2008). This type of applications often include the usage of an electromagnetic generator as the transducer, which consists of a set of coil and magnets. People have used this methods to successfully harvest energy from a wide range of applications, ranging from car suspension (Li et al., 2012) to human motion (Liu et al., 2018)

Piezoelectric materials convert mechanical strain to voltage based on the direct piezoelectric effect (Meitzler et al., 1988). This phenomenon is often found in certain crystals and ceramics. This type of transducer can take advantage of the tiny vibrations occurring on the surface of the pipelines that conveys various liquids in the oil and gas industry. Researchers have looked into and concluded that fluid flowing in conveying pipes can induce a broadband frequency vibration (Blevins et al., 1990, Sinha et al., 2005), and the turbulence in the flow can cause random pressure fluctuations on the inner surface of the pipe causing it to vibrate (Sinha et al., 2005, Pittard et al., 2004). Even though this technology is very mature, its applications are yet to be seen in the oil and gas industry, especially in the downhole environment.

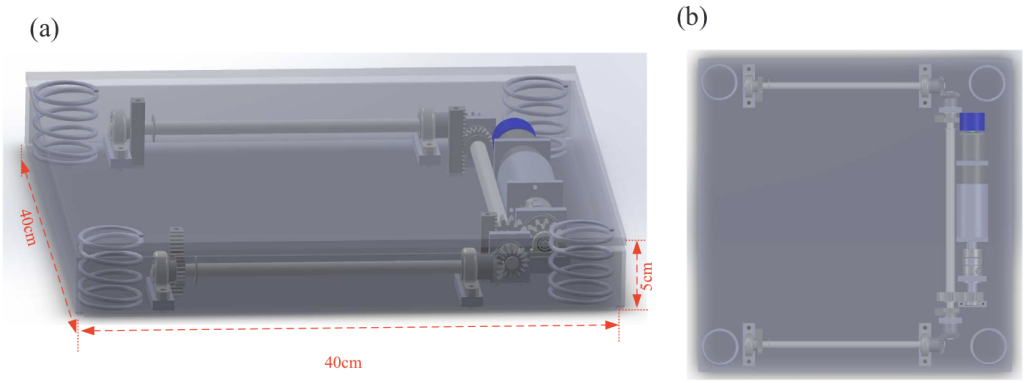

Figure 2.2: CAD DESIGN OF THE ENERGY HARVESTING PAVER (Liu et al., 2018).

2.1.3 Flow Energy

Flow energy is the most common energy source in the oil and gas industry as fluid flow is present literally through out the entire production cycles. In the well drilling phase, water is pumped through the drilling equipment to both drive and cool the drill head. In the oil extraction phase, water is pumped underground through oil injection well to pressurize the reservoir, and oil is extracted to the surface through various pumps and artificial lift. The extracted oil is transported from the well sites to the refinery and other facilities through oil pipelines, which could be as long as thousands of miles. The immense amount of energy hidden in the flows, when utilized, can be used to power a variety of applications including sensor networks and communication modules. People have primary worked on two directions when trying to harvest energy from fluid flows. The first is through various types of turbines. People have done extensive work on using turbine to extract energy from fluid flow.

The second way is to harvest energy from flow induced vibration, or vortex induced vibration. Usually a small transducer is placed in the middle of the flow. This transducer vibrates as the pressure on its surface oscillates (Niell et al., 2013). The transducer is usually designed with bluff body and a flexible piezoelectric component; the alternating stress and strain on the piezoelectric component will result in an induced voltage. An "eel" shaped piezoelectric transducer made of polyvinylidene fluoride (PVDF) was designed by Taylor et all. in 2001. an "leaf" shade piezoelectric transducer with similar principle of functionality was designed by Li and Lipson in 2009.

2.1.4 Energy Harvesting Patents

Although there is currently a lacking amount of research studies on energy harvesting in the oil and gas industry, there are several patents that try to address this challenge. Schultz et al. (2003) proposed use a flexible member to extract and amplify the flow induced vibration

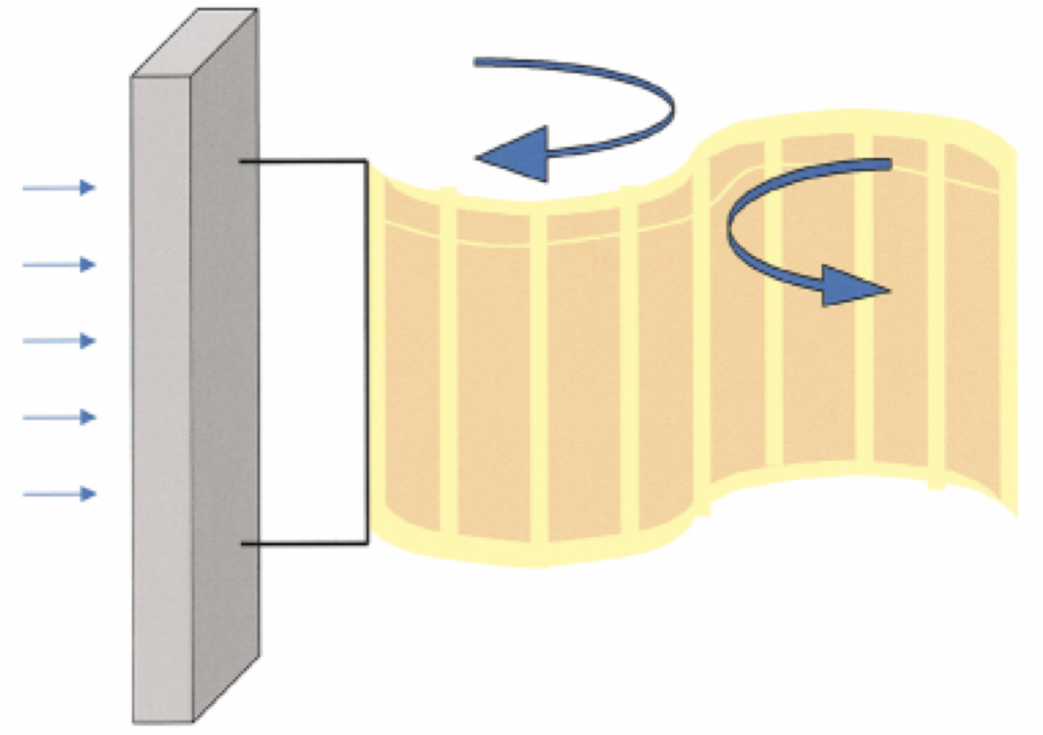

Figure 2.3: ENERGY HARVESTING EEL WITH PIEZOELECTRIC MATERIAL (Niell et al., 2013).

in downhole environment. Chen et al. (2009) proposed a membrane-based energy harvester that will oscillate with the oil flow. Luis Phillipe Tosi (2014) proposed a linear electromagnetic generator that is driven by the flow of oil production. Timothy R. Tips (2006) proposed a flow restrictive device that will alternatively increase and decrease the flow thus generating vibration for energy harvesting purpose. Tinnen et al. (2011) also proposed a flow-induced-vibration device to harvest energy in the downhole environment. Marya et al. (2011) proposed a pressure changing device to move an electrical conductor relative to a fixed magnet. Loretz et al. (2011) proposed a energy harvesting apparatus that creates mechanical motions in response to the differential pressure between hydraulically isolated zones in the oil well.

There are also several turbine-based patents related to the oil and gas industry. Schultz et al. (2005) proposed a magnetized, ring-shaped device that can be installed in the well-bore and will rotate under oil flow. Cousins (2006) proposed a positive displacement motor based energy harvester for downhole application. Schoonover (2013) proposed a retractable energy harvesting apparatus that takes advantage of the oil flow during production. Maurer et al. (2005) proposed a turbine-based energy harvester that operates near its runaway speed regardless of the load condition. There are several turbine-based patents that achieve the goal of energy harvesting through similar approaches.

2.2 Archimedean Screw Turbine

People have done extensive research on using turbines to extract energy from fluid flow. Turbines used to harvest hydropower vary in geometries and sizes. There are two main types of turbines that people commonly use.

The first type is impulse turbine, which harvests the kinetic energy of the water (U.S. Department of Energy); the runner of the turbines are driven completely by the flow of the water. The momentum of the flow transfers to the runner of the turbines, causing them to spin. The most common impulse turbines are Pelton turbines, Cross-flow turbines, and Turgo turbines. The second type is reaction turbine. This type of turbines are driven by both the pressure difference across the turbine blade surface and the motion of the water. The common types of turbines in this category includes Propellers, Francis turbines, Kaplan turbines, and Archimedean screw turbines. A more comprehensive review on the small hydropower technology can be found in the work done by Kilama in 2013.

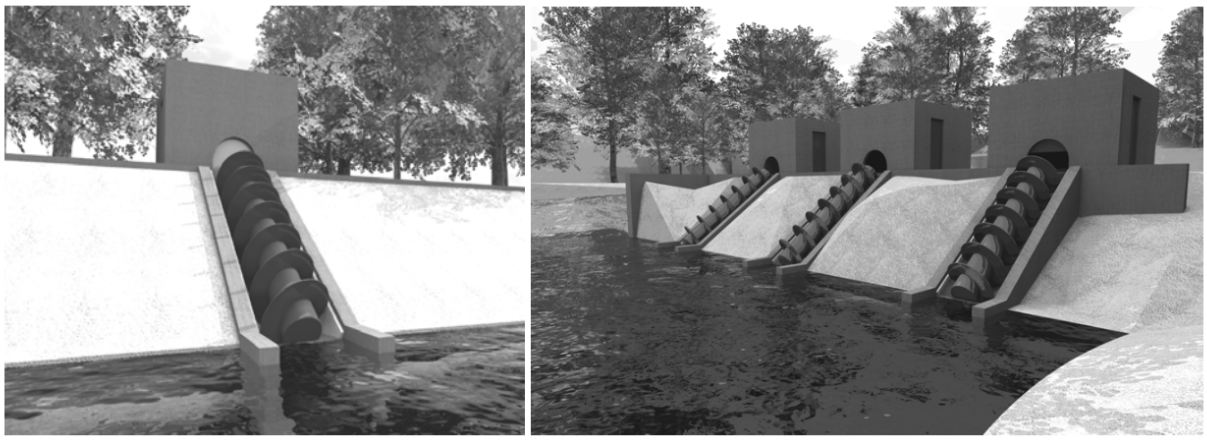

Figure 2.4: RENDERING OF ARCHIMEDEAN HYDRO PLANTS (Stergiopoulos et al., 2013).

Although Archimedean screw has a history of over 2000 years, and Archimedean screw turbines are listed as one common type of impulse turbine. The history of using Archimedean screw as a means for power generation is only around a couple of decades. The world had not seen the application of it as a turbine to generate electricity until the year of 1993 (Nuenbergk and Rorres, 2012). After the first installation in Europe, people started paying more attention to it. The number of hydroelectric plants featuring Archimedean screw turbines has increased dramatically especially in Europe (Kantert et al., 2008).

Besides lab tests, there are currently lacking number of literatures on the topic of Archimedean screw generator, at least literatures written in English. Fiardi presented a design and experiment of an Archimedean screw generator in his work in 2014. A power output of 0.098 W

was achieved. Lashofer et al., conducted a survey on plant design, cost, and operation on Archimedean screw turbine hydroelectric plants, and summarized the current state of the Archimedean screw turbine development and distribution in their paper in 2012. Haule et al., (2012) conducted experiments and concluded that Archimedean screw can maintain high efficiencies cross a wide range of flow rate.

However, the design process of the Archimedean screw turbines are still largely based on the experience with the Archimedean screw pumps. To conclude a better design approach, there were also people who looked into the modeling of the Archimedean screw turbines. Muller and Senior (2009) proposed a simplified model which links the screw efficiency to its geometry and mechanical losses. Dellinger et al. (2016) proposed a theoretical model that links the screw performance to screw geometry and flow conditions. Their model considers the various effect of leakages, friction losses and different fill levels of the screw bucket. Lubitz et al., (214) also worked on the modeling of the Archimedean screw turbines. They proposed two theoretical models based on quasi-static pressure analysis, and predict the screw performance based on various fill levels.

Compared with other types of turbines, Archimedean screw turbines have some innate advantages which make them suitable for certain site conditions. Unlike other turbines, Archimedean screw turbines only require a low head to operate (¡5m). The manufacturing cost and maintenance cost of Archimedean screw turbines are fairly low thanks to its simplistic design and geometry. One interesting characteristic that is so unique to Archimedean screw turbine is that it has the ability to allow the objects in the flow to pass through safely with hurting the screw or the objects. McNabb first conducted a study in 2003 on fish passing through Archimedean screw pumps and concluded that there was no damage done to the fish in the process. Kibel later conducted a more comprehensive study on Archimedean screw generator's ability to allow fish to pass through, and concluded that fish were able to pass through Archimedean screw generators safely. Because of this property, Archimedean screw generators are often in stalled on river and are known as fish friendly.

The characteristic of Archimedean screw turbine to allow obstacles to pass through is unique and make it the best candidate for applications in which potential objects could exist in the flow, such as in well site applications, flow can be carrying small obstacles like sand and rock debris.

2.3 Underwater Acoustic Communication

The key component to achieve underwater communication through acoustic waves is an acoustic modem, which is able to transmit and listen for acoustic signal and convert them back to digital signals. Sendra et al. compiled a list of currently available modem, both commercial and lab developed, which is shown in Figure 2.5. Commercial acoustic modems typically use a carrier frequency ranging from as low as 9 kHz to as high as 100 kHz. The

data rate varies depending on specific model, ranging from 40 *bps* up to over 30000 *bps*. Although the deployment environment can change drastically, most modems are designed and rated for open water usage, with a maximum data transmission distance from 100 m, to up to 6000 m. This distance rating is enough for well site application since typical oil wells are within 6000 m depth range. All modems are equipped with three power modes, transmitting (TX), receiving (RX), and idle. The idle power consumption is pretty low across all brands and models, ranging from as low as 1 mW, to as high as 40 mW. The receiving (RX) power consumption is higher than the idle power consumption, ranging from 60 mW to 1.8 W, which are still pretty low. The major power usage occurs when the modem is actively transmitting data. Depending on the models, this transmitting (TX) power consumption can reach as low as 1 W, or as high as 300 W. Although there does not seem to be a clear correlation between the power consumption and the maximum transmitting distance or the carrier frequency, the maximum transmission distance appears to decrease exponentially as the carrier frequency increases across all commercial devices (Figure 2.6). This agrees with the understanding that the attenuation of acoustic waves is proportional to the frequency of the wave.

There have been many under water acoustic modem developed in the past decade. Each of them feature some unique characteristics. Sanchez et al. developed an acoustic modem featuring ultra-low power consumption with an idle power consumption of 3 μW, a receiving power consumption of 24 mW, and a transmitting power consumption of 12 mW. With such a low power consumption, they managed to reach a maximum transmission distance of 100 m.

Although acoustic communication in water-filled pipes is yet to be seen in the real-world application or literatures, there have been researches that looked into similar concept. One major topic related to acoustic wave propagation in water-filled pipes is leakage detection. Long et al. (2003) looked into the fundamental modes of acoustic wave propagating in buried iron water pipes, and the mode attenuation resulted from the leakage into the surrounding environments. Baik et al (2010). looked into the modeling and experiments of acoustic attenuation in liquid-filled pipes. Graf et al. (2014) investigated the same problem from an FEA perspective.

Underwater Acoustic Modem	Modulation	Carrier Frequency	Bandwidth	Data rate	TX Power consumption	RX Power consumption	Idle Power consumption	Max. distance
DEVICES DEVELOPED BY RESEARCH GROUPS								
[5]	FSK	320 Hz and 10 kHz	1 kHz	96 bps and 2400 bps	12 mW	24 mW	3 µW	100 m
[19]	n/a	n/a	n/a	1-10 Mbps	n/a	n/a	n/a	100 m
[25]	FSK	35 kHz	6 kHz	200 bps	750 mW		35 mW	350 m
[27]	KSK	85 kHz	n/a	1 kbps	108 mW	24 mW	8.1 µW	240 m
[28]	n/a	9-14 kHz	75 kHz	1.2 kbps	n/a	n/a	n/a	2000 m
[21]	BPSK	80 kHz	n/a	80 kbps	n/a	n/a	n/a	50 m
[30]	FSK	30 kHz	n/a	300 bps	n/a	n/a	n/a	400 m
[32]	FSK	9 kHz	n/a	1900 bps	n/a	n/a	n/a	200 m
COMMERCIAL DEVICES								
Aquatec AQUAModem 1000 [36]	n/a	9.75 kHz	4.5 kHz	2000 bps	20 W	0.6 W	1 mW	5000 m
DSPComm AquaComm Marlin [37]	n/a	23 kHz	14 kHz	480 bps	1.8 W	0.252 W	1.8 mW	1000 m
DSPComm AquaComm Mako [38]	n/a	23 kHz	14 kHz	240 bps	1.8 W	0.252 W	1.8 mW	100 m
DSPComm AquaComm Orca [37]	n/a	14 kHz	100 kHz	0.007 bps	0.252 W	1.8 W	25.2 mW	3000 m
Desert Star Systems SAM-1[38]	n/a	37.5 kHz	9 kHz	154 bps	32 W	0.168 W	n/a	1000 m
EvoLogics S2CR 48/78USBL [39]	n/a	48-78 kHz	30 kHz	31200 bps	18 W	1.1 W	2.5 mW	1000 m
EvoLogics S2CR 40/80 USBL [39]	n/a	38-64 kHz	26 kHz	27700 bps	40 W	1.1 W	2.5 mW	1000 m
EvoLogics S2CR 18/34wise [39]	n/a	18-34 kHz	16 kHz	13900 bps	35 W	1.3 W	2.5 mW	3500 m
EvoLogics S2CR 12/24 USBL [39]	n/a	13-24 kHz	11 kHz	9200 bps	15 W	1.1 W	2.5 mW	6000 m
EvoLogics S2CR 7/17 USBL [39]	n/a	7-17 kHz	10 kHz	6900 bps	40 W	1.1 W	2.5 mW	8000 m
LinkQuest UWM1000 [40]	n/a	35695 kHz	17.85 kHz	17800 bps	1 W	0.75 W	8 mW	3500 m
LinkQuest UWM2000 [40]	n/a	35695 kHz	17.85 kHz	17800 bps	2 W	0.8 W	8 mW	1500 m
LinkQuest UWM2000H [40]	n/a	35695 kHz	17.85 kHz	17800 bps	2 W	0.8 W	8 mW	1500 m
LinkQuest UWM2200 [40]	n/a	71.4 kHz	35.7 kHz	35700 bps	6 W	1 W	12 mW	1000 m
LinkQuest UWM3000 [40]	n/a	10 kHz	5 kHz	5000 bps	12 W	0.8 W	8 mW	3000 m
LinkQuest UWM3000H [40]	n/a	10 kHz	5 kHz	5000 bps	12 W	0.8 W	8 mW	3000 m
LinkQuest UWM4000 [40]	n/a	17 kHz	8.5 kHz	8500 bps	7 W	0.8 W	8 mW	4000 m
LinkQuest UWM10000 [40]	n/a	10 kHz	5 kHz	5000 bps	40 W	0.8 W	9 mW	1000 m
Teledyne Benthos Atm9xx [41]	PSK	11.5 kHz 18.5 kHz 24.5 kHz	5 kHz	15360 bps	20 W	0.768 W	16.8 mW	6000 m
Teledyne Benthos Atm9xx [41]	MFSK	11.5 kHz 18.5 kHz 24.5 kHz	5 kHz	2400 bps	20 W	0.768 W	16.8 mW	6000 m
Teledyne Benthos Atm88x [41]	PSK	11.5 kHz 18.5 kHz	5 kHz	15360 bps	84 W	0.756 W	16.8 mW	6000 m
Teledyne Benthos Atm88x [41]	FSK	11.5 kHz 18.5 kHz	5 kHz	2400 bps	84 W	0.756 W	16.8 mW	6000 m
TriTech MicronModem [42]	n/a	22 kHz	4 kHz	40 bps	7.92 W	0.72 W	n/a	500 m
uComm Underwater Acoustic Modem [43]	n/a	26 kHz	n/a	9000 bps	40 W	60 mW	3 mW	3000 m
AM-OFDM-S [44]	OFDM	21-27 kHz	n/a	1600 bps	5-20 W	0.7W	0.13 mW	4000 m
MATS 3 G 12 KHZ [45]	n/a	10-15 kHz	n/a	Up to 7400 bps	75 W	0.6 W	40 mW	15 Km
GPM 3000 Acoustic Modem [46]	DSSS	n/a	n/a	Up to 1200b•s	300W	1.8 W	0.08 W	25 Km

Figure 2.5: COMPARISON OF ACOUSTIC MODEMS (Sendra et al., 2016).

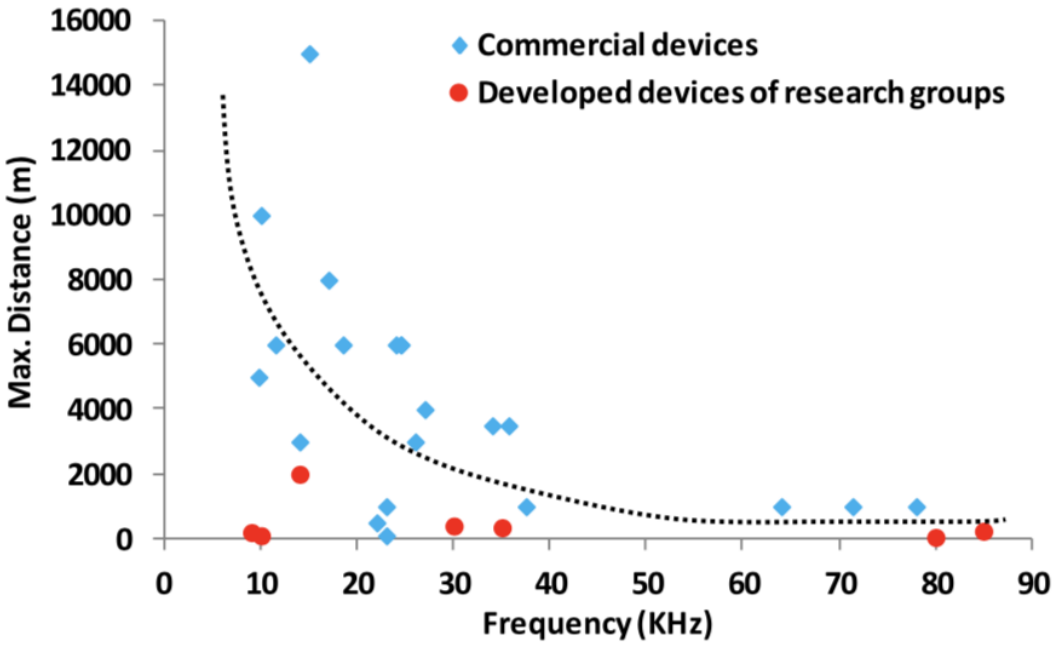

Figure 2.6: RELATIONSHIP BETWEEN WORKING FREQUENCY AND MAXIMUM DISTANCE (Sendra et al., 2016).

Chapter 3

Harvester Design and Optimization

This chapter goes through the design process of the AST based energy harvester, including the working principle and the design optimization. Optimization was done through parametric study using Ansys Fluent, in which, the optimal geometry and operating condition were analyzed.

3.1 Design and Working Principle

Archimedean screw turbines have the innate advantages compared to other turbines. Previous studies done by other researchers have shown that Archimedean screw turbines are suitable for low flow and low head, even zero head situations. Archimedean screws also have the quality to allow objects, such as fish in river, to pass by safely, which makes it very environmentally friendly and very suitable for river applications. Due to Archimedean screw turbine's simplistic structure, the manufacturing and maintenance cost is very low compared to other types of turbines. Because of these qualities, Archimedean screw turbines might be the perfect solution to harvest energy from various pipes in oil and gas industry.

Figure 3.1 shows the CAD model of the designed energy harvester. The design of the harvester consists of three parts. The top part is the generator and generator casing. Generator's main function is electricity generation. the casing secures the generator in place and waterproofs it, ensuring the generator's functionality under submerged conditions. The bottom part is the Archimedean screw turbine, which extracts mechanical energy from the flows and transmits it to the generator. The Archimedean screw has a long profile compared to other traditional turbines, with two spiral blades running along its cylindrical cord. Both the generator and AST are inclosed and supported by a cylindrical outer casing. The cylindrical casing is composed of five segments to allow easy assembly. Two of the segments are embedded with bearings to ensure that the AST and the generator are co-axial and can operate smoothly. these two segments also function as the connection units of the other

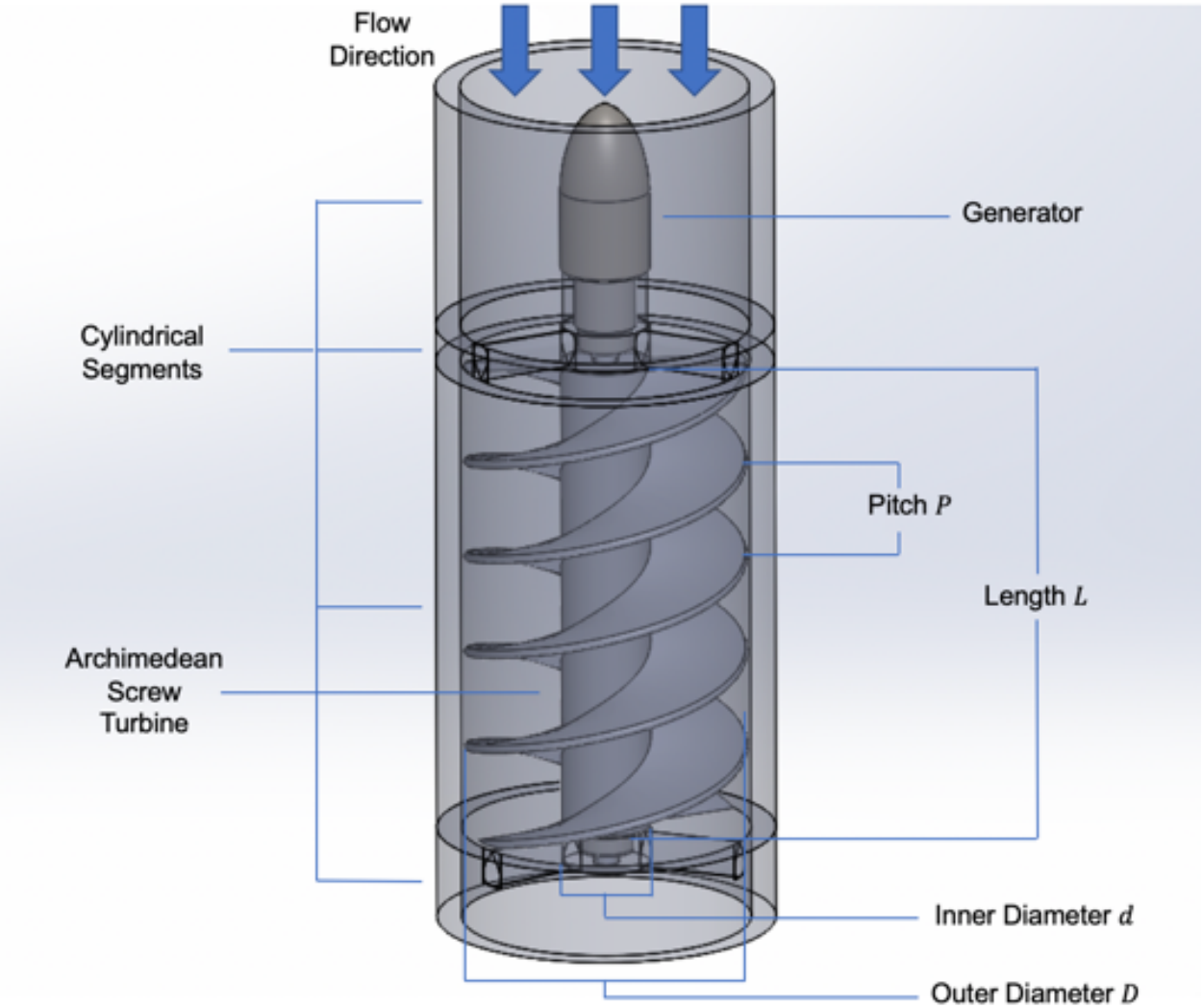

Figure 3.1: 3D ILLUSTRATION OF THE DESIGNED HARVESTER.

three segments, holding the entire system together. The harvester is designed to replace, or installed inside a segment of the pipe used in the oil production cycle, so that the existing equipments can be retrofitted with the harvester.

In the oil production cycle, fluid is pumped through various pipes. This study mainly focuses on the beginning part of the oil production, which is water injection where water is pumped into the ground through injection wells. During this process, water running across the AST will induce a pressure difference between the opposite sides of the helical blades, creating a driving torque that rotates the AST. This torque further drives the connected generator on the top to generate electricity. To maximize the power generation of the harvester, several design optimizations need to be made. These include the optimization of the AST structure, and the optimization of the generator. Since the study does not include the generator design,

a commercial generator will be used.

3.2 Parametric Study with CFD Simulations

Since the pipe flow is assumed to be under steady state, the system will be operating under constant conditions, meaning constant velocity. Since there is no angular acceleration, and the system does not have a inatia term, the motion of the generator can be simplified as the following.

$$(c_m + c_e)\dot{\theta} + \tau_f = \tau$$

where c_m and c_e are respectively the mechanical damping and electrical damping associated with the system, τ is total torque generated by the AST under flow condition, τ_f is the friction induced torque which is constant and only associated with the rotational direction of the AST. The power output of the generator can be expressed as the following.

$$P = (\tau - \tau_f - c_m\dot{\theta})\dot{\theta} = c_e\dot{\theta}^2$$

The value of friction τ_f and the mechanical damping c_m are unknown but non-varying. It's easy to see that the power generation of the system is associated with the torque generation of the AST τ, the operating speed $\dot{\theta}$, and the electrical damping of the generator c_e To maximize the generated power, it is crucial to first, optimize the AST's torque generation and operating speed to yield the most power output. Second, to choose a generator that has the corresponding electrical damping to match the optimal rotational speed $\dot{\theta}$.

With this purpose in mind, parametric studies were carried out to determine the optimal geometry and operating conditions of such system. The commercial CFD software Ansys Fluent was used for the numerical analysis to study the performance of the AST. The CFD settings used in Ansys Fluent is summarized below.

- Semi-Implicit Method Pressure Linked Equ (SIMPLE)
- Second order up-wind discretization
- K- ϵ turbulence model
- Convergence: $10^{-}5$ of initial residuals
- 0.5 m/s velocity inlet

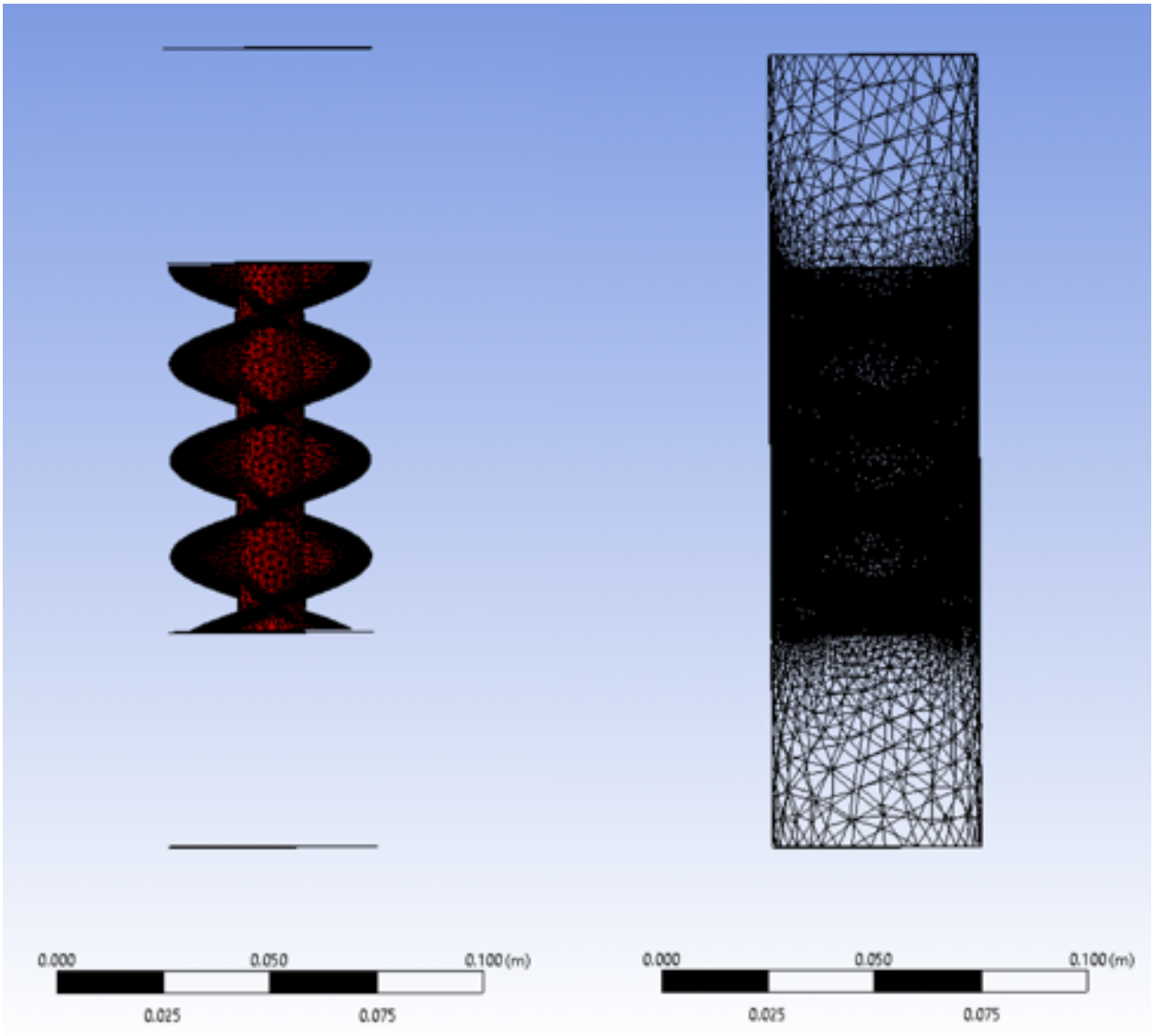

Figure 3.2: MESH USED FOR CFD SIMULATION.

3.2.1 Geometric Optimization

The main parameters that affect the performance of an AST are the flow rate Q, the screw length L, the screw pitch P, the outer diameter D, the inner diameter d,the number of blades N, and the rotational speed of the screw $\dot{\theta}$. CFD simulations were conducted in order to determine the optimal geometry of the AST . For this particular application, the AST was designed to have an outer diameter of 50 mm to fit in a typical water injection well with a diameter of 52 mm. To achieve maximum efficiency, the gap between the pipe and the AST should be kept as small as possible. The AST has one to two helical blades running through

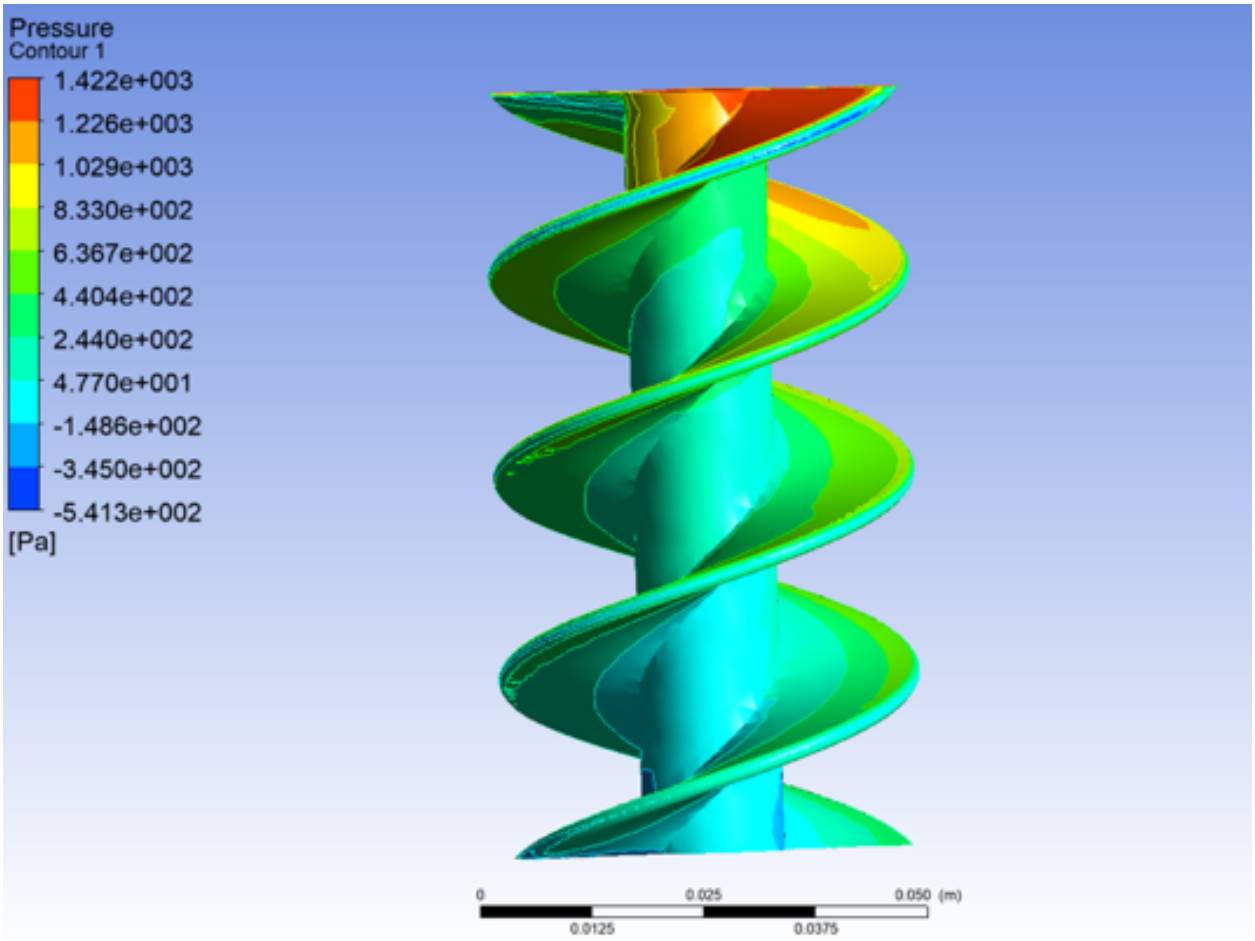

Figure 3.3: PRESSURE CONTOUR ON THE AST.

the entire length and an inner diameter of 16 mm. The remaining geometric parameters of the AST need to be optimized based on the flow condition of the specific water injection well.

With diameters of the AST being fixed, three parameters, number of blades N, screw length L, and screw pitch P, were varied in the optimization process. Screw length L was varied between 65 mm and 135 mm with 10 mm increment. Screw pitch was varied between 25 mm and 75 mm with 5 mm increment. Table 3.1 summarizes the parameters used in the CFD simulation.

Each AST geometry was simulated under a fixed flow rate of 0.95 L/s, equivalent to 0.5 m/s in terms of flow velocity, which corresponds to a typical flow rate of a water injection well. To study the performance of each screw configuration, the AST was fixed in place, ie 0 RPM rotational speed. Preliminary study was conducted to study the effect of the number of blades on the torque generation. In these simulations, screw length was kept at 85 mm and

Table 3.1: PARAMETERS USED IN CFD SIMULATION.

Parameter	Meaning	Value
Q	Flow rate	$0.95L/s(0.5m/s)$
D	AST outer diameter	$50mm$
d	AST inner diameter	$16mm$
N	Number of blades	$1-3$
D_p	Pipe diameter	$51mm$
L	Screw length	$65mm-135mm$
P	Screw pitch	$25mm-75mm$

the screw pitch was kept at 45 mm. Figure 3.4 shows the simulation result. The single blade design has the lowest torque generation, and the two blade design and three blade design have comparable results with the two blade design having slightly higher torque generation.

The rest of the parametric study was conducted using a AST design with two blades; screw length and screw pitch were varied in the rest of the simulations. Figure 3.5 shows the torque generated by the AST. The result suggests that the generated torque is positively proportional to the screw length and negatively proportional to the screw pitch. The screw pitch appears to be the major factor in terms of the torque generation. A 53% decrease in screw pitch can result in a maximum of 114% increase in the torque generation. Although the increased length did result in an increased torque generation, the effect is minimal. A 108% increase in screw length only results in a maximum of 25% increase in the torque generation. This result suggests that in order to maximize the torque generation, an AST with longer length and smaller pitch is desired for this particular application. The maximum torque generated in the CFD simulation is 44.5 mNm, which occurs when the screw length is 135 mm and the screw pitch is 25 mm.

3.2.2 Optimal Operating Condition

Turbine geometry is not the only deciding factor that determines how much torque an AST can produce; it also heavily depends on the operating speed of the AST. Hence, CFD simulation was also carried out under different rotational speeds to calculate the expected power output. Such information is crucial in terms of determining the optimal operating range of the AST and generator selection in order to maximize both the mechanical efficiency and the electrical efficiency of the system.

The power output is calculated as the following,

$$Power = \tau_{AST} \times \dot{\theta}_{AST}$$

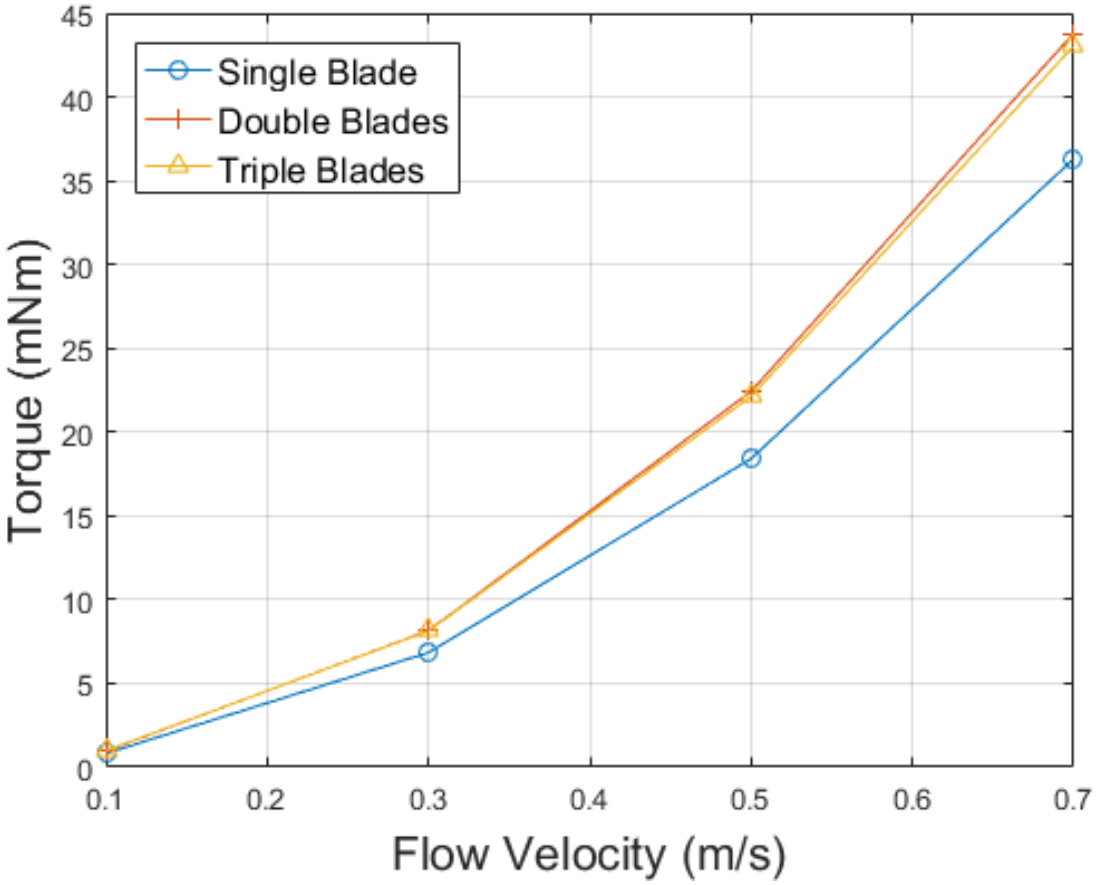

Figure 3.4: TORQUE GENERATION OF SCRES WITH DIFFERENT BLADE NUMBERS AT 0 RPM.

where τ_{AST} is the torque generated by the AST and $\dot{\theta}_{AST}$ is the rotational speed of the AST. Figure 3.6 - figure **??** present the simulated power output of different screw geometries under various operating conditions ranging from 0 RPM to 600 RPM with a constant water flow rate of 0.95 L/s.

With a configuration of 45 mm pitch, the power output increases as the screw length increases under the same operating RPM. This is expected because a longer screw will have a larger capacity to carry more water inside. For screw with the same length, the power output increases as the rotational speed increases until it reaches the optimal rotational speed. In this case, this optimal rotational speed is 350 RPM. After that, the power output of the AST starts to decrease. For 45 mm pitch AST, the simulated maximum power output is 0.43 W, which occurs when the screw length is 135 mm, and the rotational speed is 350 RPM. However the screw length appears to have small to no effect on the the optimal rotational speed; for 45 mm pitch screws, screws with lengths varying between 65 mm to 135 mm all

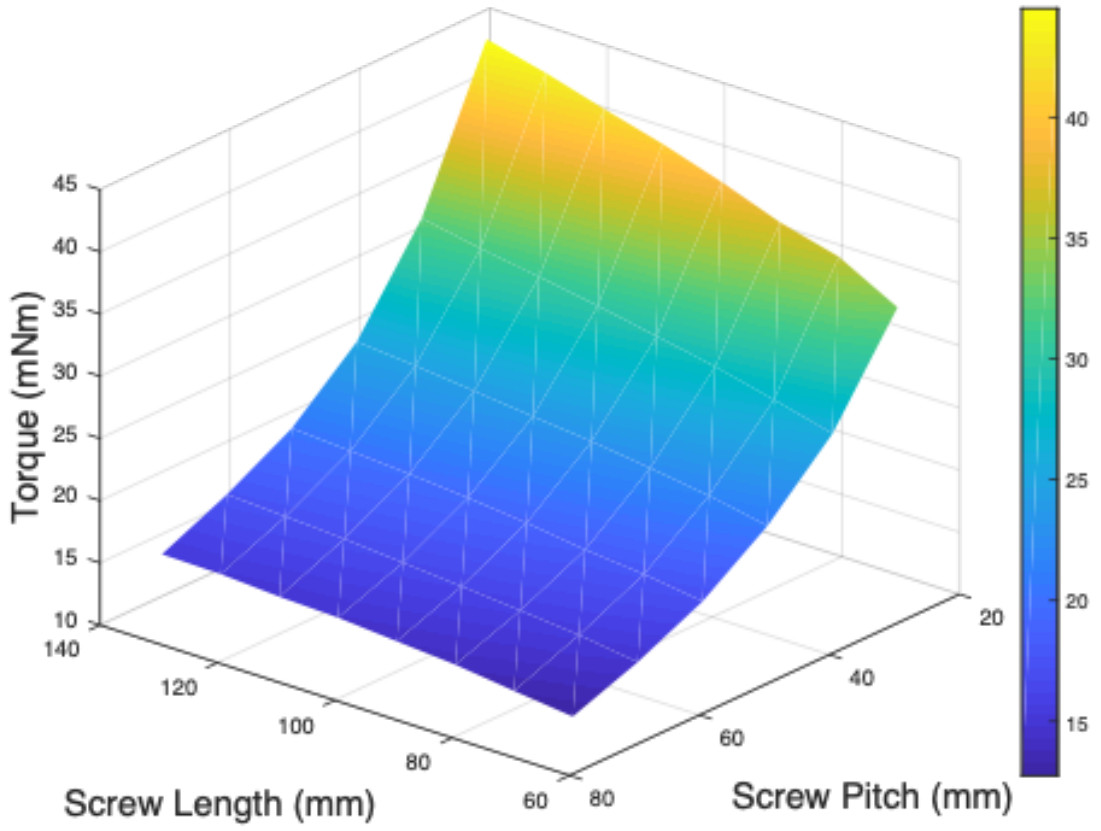

Figure 3.5: TORQUE GENERATION OF VARIOUS SCREW GEOMETRIES AT 0 RPM.

have an optimal rotational speed of 350 RPM.

This trend continues exhibit in other pitch ranges,35 mm, 55 mm, 65 mm, and 75 mm. For a 35 mm configuration, the maximum power output was 0.66 W, which occurred when the screw has a length of 135 mm and was operating at 450 RPM. For a 55 mm configuration, the maximum power output was 0.30 W, which occurred when the screw has a length of 135 mm and was operating at 300 RPM. For a 65 mm configuration, the maximum power output was 0.22 W, which occurred when the screw has a length of 135 mm and was operating at 250 RPM. For a 75 mm configuration, the maximum power output was 0.17 W, which occurred when the screw has a length of 135 mm and was operating at 200 RPM.

The results suggest that there is a single optimal rotational speed associated with each screw pitch. As the screw pitch increases, the corresponding optimal rotational speed decreases. There are no observable correlation between the optimal rotational speed and the screw length; the the optimal rotational speed remains the same for ASTs across all length range

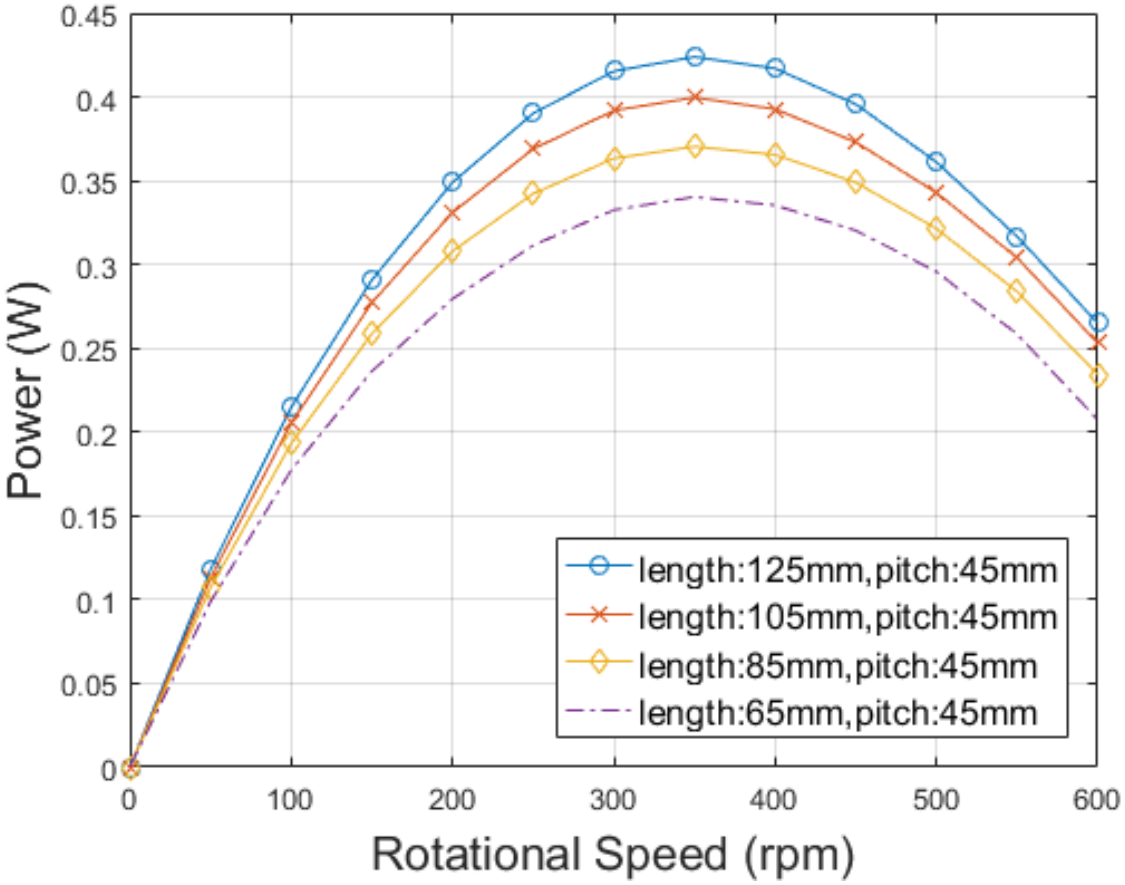

Figure 3.6: POWER OUTPUT OF SCREW WITH 35 MM PITCH.

with same pitch,

From the simulation, ASTs with pitches ranging from 35 mm to 75 mm have an optimal rotational speed ranging from 450 RPM to 200 RPM. Table 3.2 summarized the optimal operating speed for ASTs with different configurations.

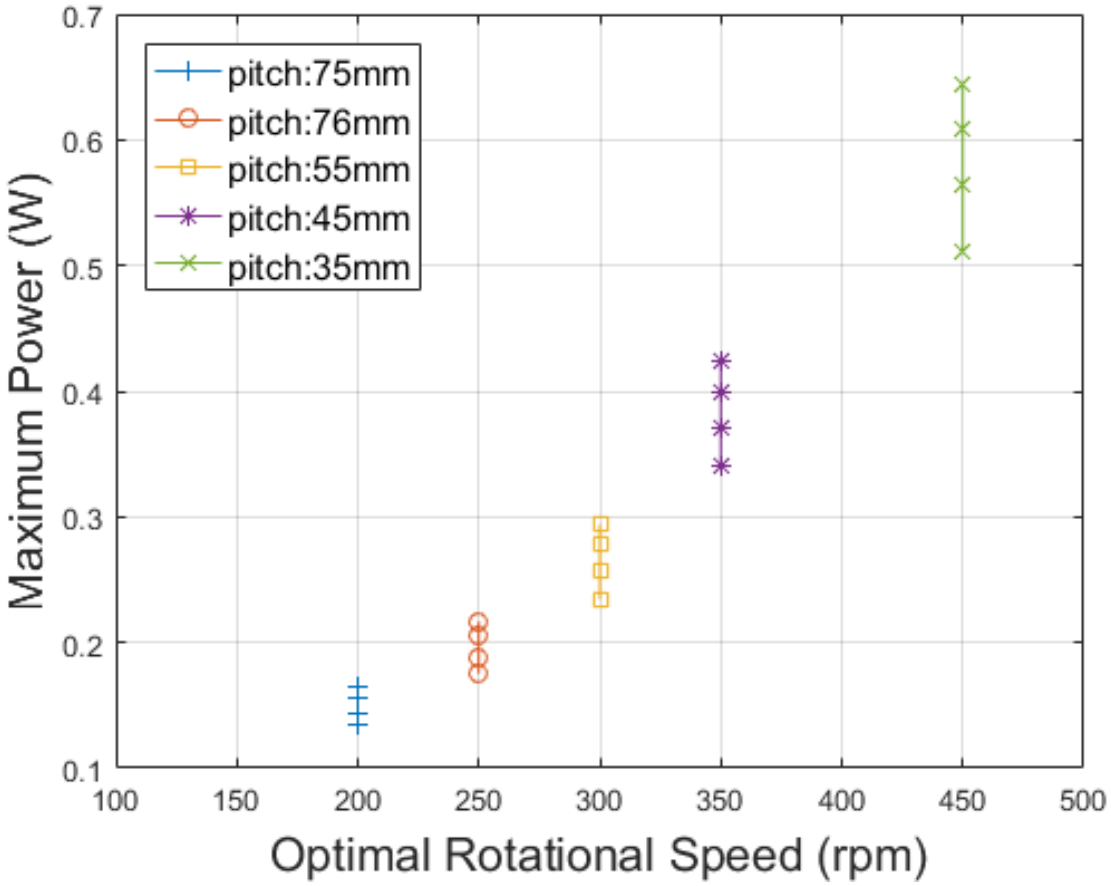

Figure 3.7: OPTIMAL ROTATIONAL SPEED OF ASTs WITH DIFFERENT PITCHES (LENGTH ARE VARIED FROM 65 MM TO 135 MM FOR EACH PTCH WITH OUTPUT POWER PROPORTIONAL TO THE LENGTH).

Table 3.2: OPTIMAL RPM FOR DIFFERENT PITCHES.

Pitch	Speed
75 mm	200 rpm
65 mm	250 rpm
55 mm	300 rpm
45 mm	350 rpm
35 mm	450 rpm

Chapter 4

Acoustic Wave Simulation

Acoustic modems and acoustic communications are most commonly used in open water environments. Whether such technology is feasible in oil and gas industry is determinant on the performance of acoustic communication in liquid filled pipes. The performance of acoustic communication was studied by investigating the attenuation of acoustic wave propagating in said pipes. This part of study was carried out using commercial software $COMSOLMultiphysics$. This chapter goes through the FEA simulations of acoustic waves propagating in water-filled pipes.

$COMSOLMultiphysics$ is an FEA software with different modules, suitable for FEA simulations for applications such as fluid, stress, magnetic field, and etc. In this particular study, the Acoustic - Structure Interaction Module was used. The simulating process follows the similar approach done by Graf et al. (2014). In the FEA simulation, the pipe wall is modeled as an elastic layer, governed by the following equation.

$$\frac{\partial^2 \vec{u}}{\partial t^2} - c_1^2 \nabla(\nabla \vec{u}) + c_2^2 \nabla \times (\nabla \times \vec{u}) = 0$$

c_1^2 is defined to be

$$\frac{\lambda_L + 2\mu_L}{\rho}$$

and c_2^2 is defined to be

$$\frac{\mu_L}{\rho}$$

where λ_L and μ_L are the Lame constants and ρ is the material density.

The water in the pipe and the surrounding soils are modeled as fluids, which is governed by the following Helmholtz equation for the pressure field.

$$\nabla(\frac{1}{\rho}\nabla p) - \frac{1}{\rho c^2}\frac{\partial^2 p}{\partial t^2} = 0$$

where c is the sound velocity and ρ is the fluid density in the respective media. These two equations are coupled and solved to get the pressure filed results. The interaction between the fluid domain and elastic layer are governed by the boundary conditions in the following equations.

$$-\vec{n}\frac{1}{\rho}\nabla p = \vec{n}\frac{\partial^2 \vec{u}}{\partial t^2}$$

$$\underline{\underline{\sigma}} \cdot \vec{n} = p\vec{n}$$

where $\vec{n}$ is the unit vecter perpendicular to the elastic layer and $\underline{\underline{\sigma}}$ is the stress tensor in the elastic material. For a more comprehensive theory of acoustic and elastic waves, refer to the book *BasicLinearAcoustics*, by Pierce, A.D.

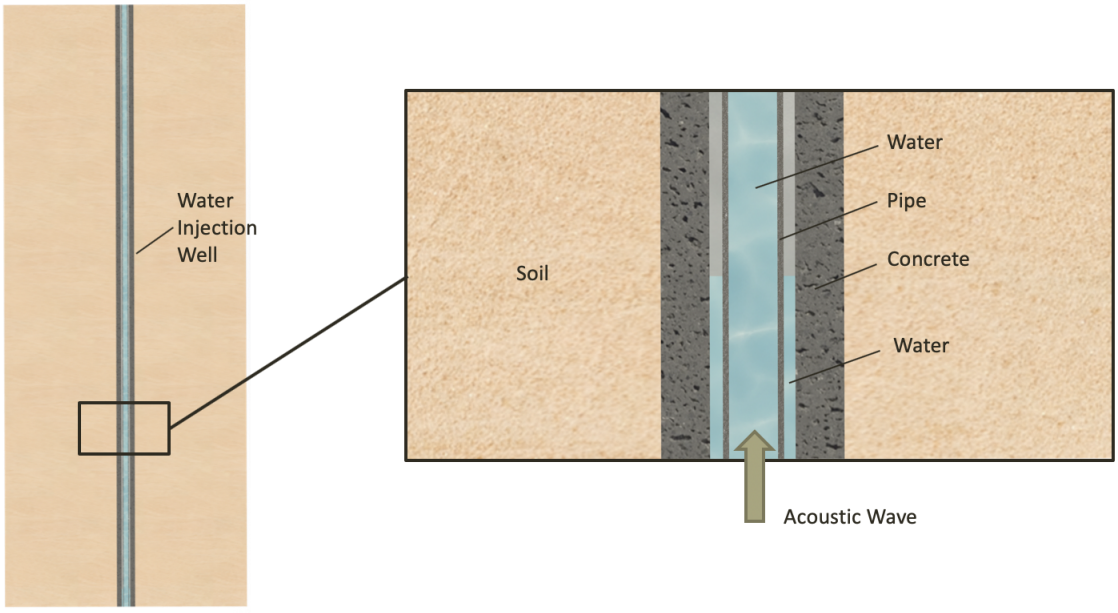

Figure 4.1: Illustration of A Water Injection Well.

Table 4.1: MATERIAL PROPERTY USED IN COMSOL FEA SIMULATION.

Material	Property	Value
Water	Density ρ	$1000kg/m^3$
	Sound speed c	$1481m/s$
Steel	Density ρ	$7850kg/m^3$
	Sound speed c	$5790m/s$
Concrete	Density ρ	$2400kg/m^3$
	Sound speed c	$3500m/s$
Soil	Density ρ	$2500kg/m^3$
	Sound speed c	$1000m/s$

4.1 Attenuation in Pipe

Figure 4.1 shows an illustration of a water injection well. The typical diameter of a water injection well is 5.2 cm and the length can be as long as thousands of meters. These wells in the oil field can all be simplified and treated as fluid filled pipes buried in soil. FEA analysis was carried out using Commercial software $COMSOLMultiphysics$ to simulate the propagation and attenuation characteristics of acoustic waves in such pipes.

Because of the limitation of computational power, it is unfeasible to simulate a pipe that's is too long. For this reason, the distance of the simulated acoustic wave propagation was caped at 10 m. The structure of a water injection well and its surrounding environment were recreated in $COMSOL$. Due to the slender profile of the structure, only the top and bottom portions are showing in the illustrations (Figure 4.2) to be able to show each layer more clearly; the middle portion connecting the top and bottom is omited. Because of the symmetric nature of the structure, the well and surrounding environment were created in a symmetric 2D frame. The inner most layer is the water in the pipe, which is represented by a 6-cm-diameter cylinder. The water later is bounded by the 5-mm-thick pipe, which is bounded by another 2-cm water later. The pipe is supported by a cylindrical concrete layer. The entire structure is bounded by soils. The outer most is the Perfectly Matched Layers (PML), which terminates the acoustic simulation in both the axial and radial direction. The mesh size used in the simulation was limited to a maximum size of 1/5 of the wave length depending on which media the acoustic wave is propagating through. The material used in the simulated were pulled from the standard $COMSOL$ database. The material properties are summarized in Table 4.1.

An acoustic wave is generated by applying an acoustic pressure with an intensity of 185 dB at one end of the pipe, which equals to the transmitting intensity of a typical acoustic modem. The frequency of the acoustic wave is chosen to be 38.7 kHz to match the working frequency of a typical underwater acoustic modem. Figure 4.3 shows the simulation result

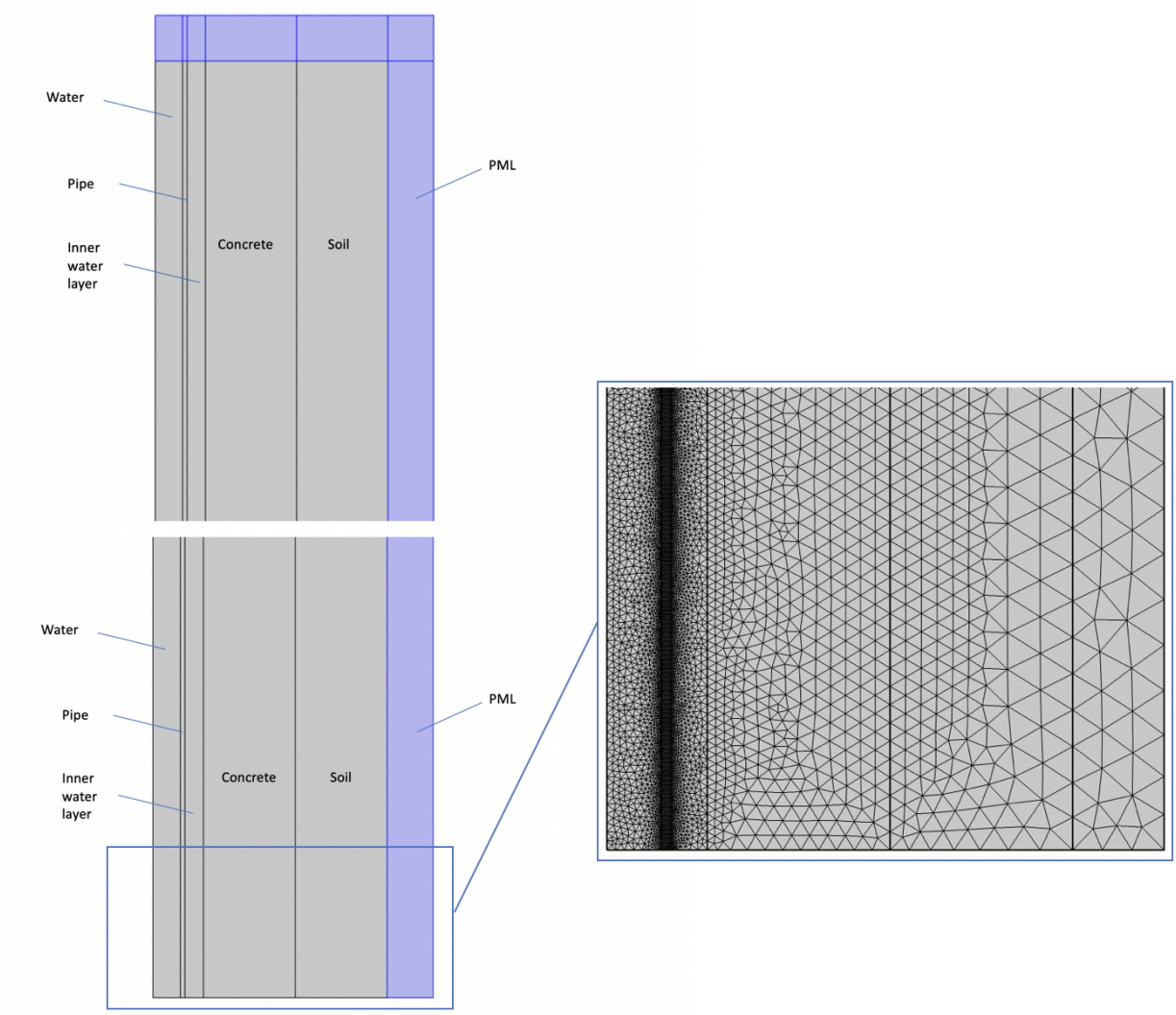

Figure 4.2: WELL GEOMETRY USED IN COMSOL FEA SIMULATION.

of acoustic intensity in dB vs the distance in m as the acoustic wave propagates through the pipe. The red curve represents the high intensity acoustic wave propagating in the water-filled pipe. The green and blue curves with lower intensity represent the acoustic waves induced by vibration due to acoustic-structure interaction in the steel pipe and the surrounding environments. These induced acoustic waves are the sources of the energy leak and are the reason of the acoustic attenuation in the pipe.

The result shows a attenuation of approximately 30 dB over the 10 m distance. The intensity of acoustic waves propagating in any media decay exponentially, which means that the acoustic attenuation will be linear in dB scale. Thus, attenuation of the simulated acoustic propagation can be approximated to be 3 dB/m. This attenuation is due to the energy loss

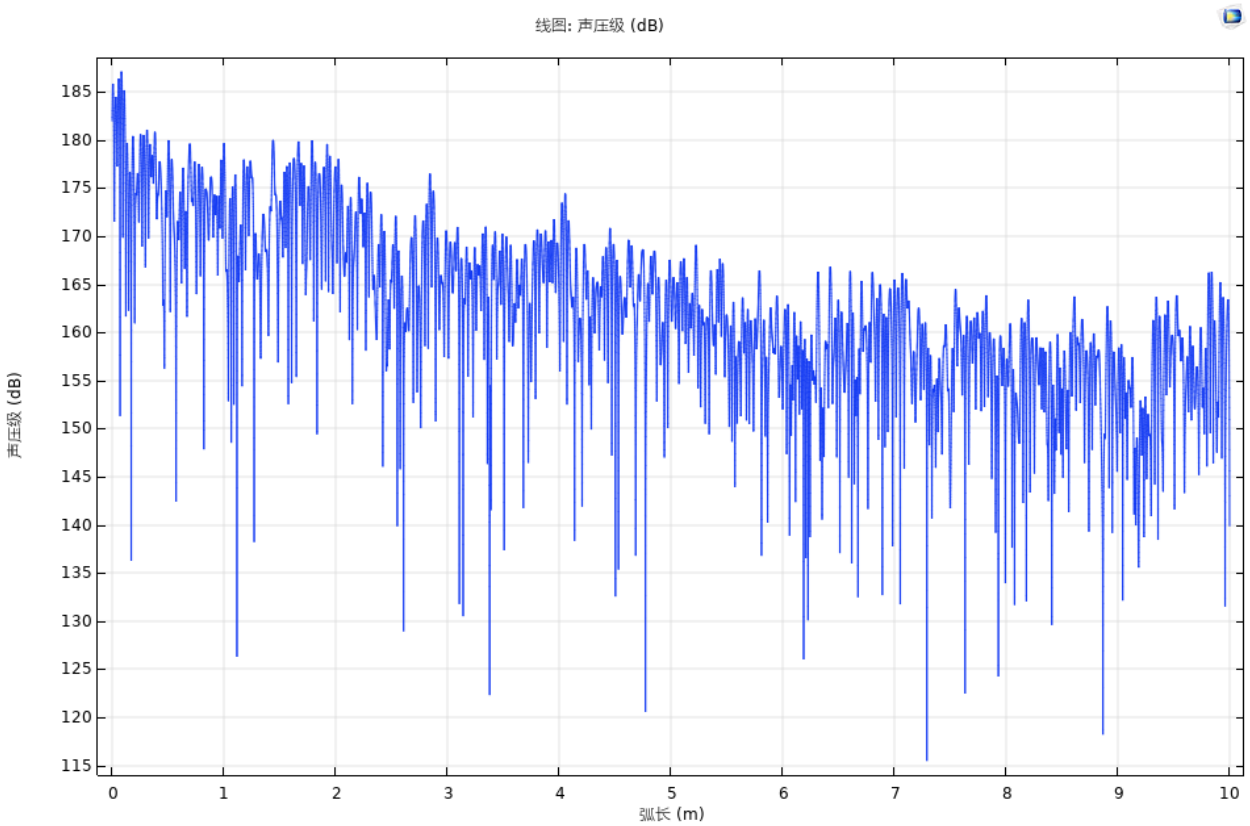

Figure 4.3: ACOUSTIC INTENSITY VS PROPAGATION DISTANCE FOR 38.7 kHz WAVE.

to the pipe wall and then radiating into the surrounding environments. Figure 4.4 shows the induced vibration in the surrounding environments.

Underwater acoustic modems have a receiving threshold, which corresponding to the minimum intensity required for any acoustic signal to be received successfully. This thresholds varies depending on the model of the modem and the setting for a particular environment. For most acoustic modems available in the market, this threshold typically varies between 85 dB for quiet environments, such as lakes and deep water, and 125 dB for noisier environments, such as harbor or places near hydraulic equipments. Using the threshold of 125 dB for our application, with an attenuation of 3 dB/m, the acoustic modems can support a communication distance of 20 m, which is not sufficient for oil field downhole applications.

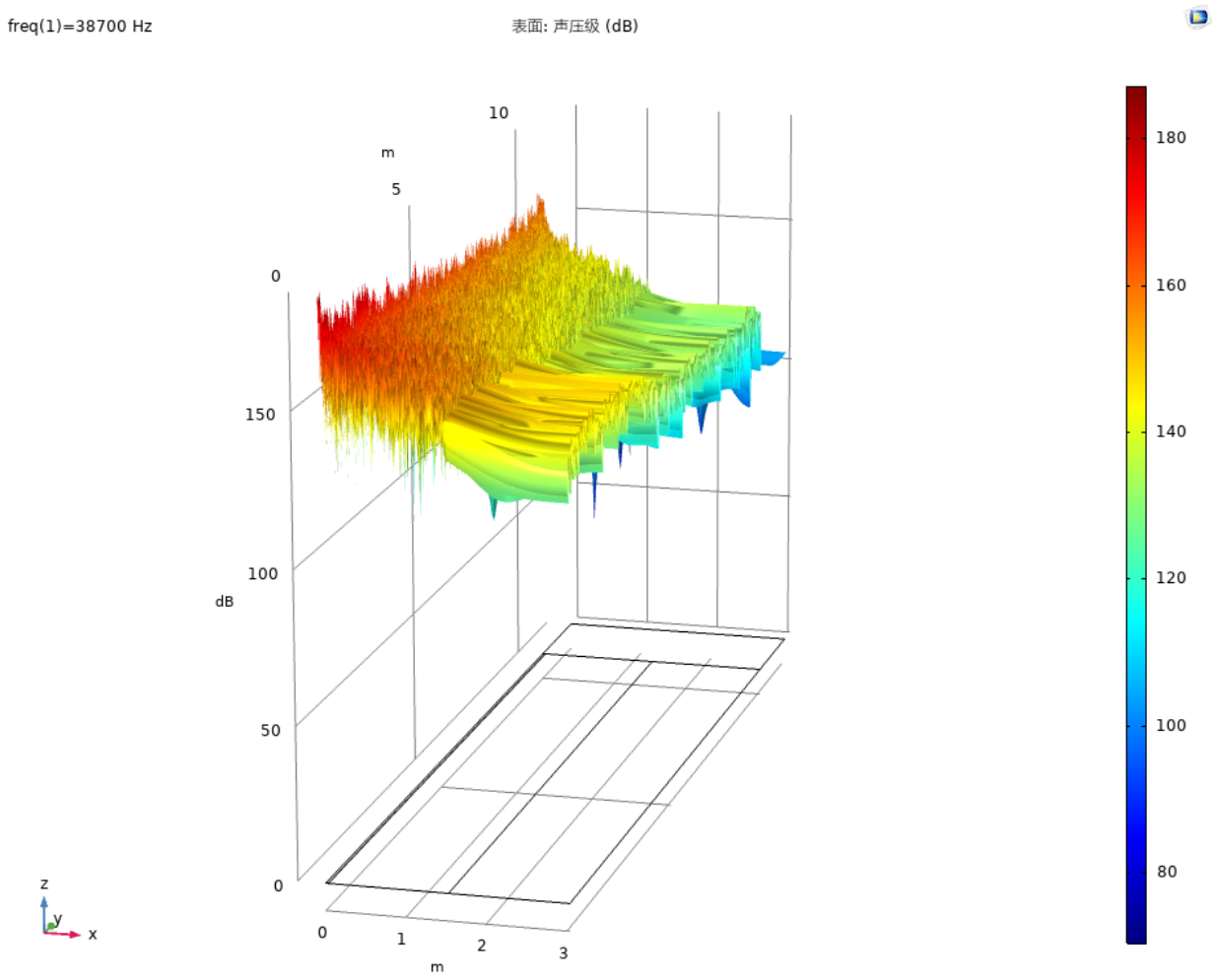

Figure 4.4: VIBRATION INDUCED IN SURROUNDING ENVIRONMENT FOR 38.7 kHz WAVE.

Chapter 5

Lab Test and Acoustic Communication

Although the results from CFD simulation suggest that a long screw with small pitch will yield the best power output, there are other factors that need to be considered. Due to the small size of the AST and the complex conditions of the downhole environment, the profile of the harvester needs to be as small as possible while meeting the power generation requirement. The total length of the harvester was kept relatively short according to the requirement of the oil company. The pitch of the AST wasn't decreased to the extreme so that potential obstacles, such as sand and tiny rocks, can safely pass through without blocking the pipes or wells. As a result, the final geometry of the AST was designed to have a length of 85 mm and a pitch of 45 mm. The AST has an inner diameter of 8 mm, an outer Diameter of 50 mm, with two helical blades running through the entire length. The gap between the AST and the pipe wall was kept around 1 mm to allow some manufacturing tolerance. The specifications of the AST are listed in Table 5.1. A CAD model of the design was first created with the help of commercial CAD software SolidWorks. The prototype was then fabricated using a SLA 3D printer (Form 2) from Formlabs. Figure 5.1 and Figure 5.2 show the printed prototype. This chapter goes through the lab testing process for both the power generation and acoustic communication.

5.1 Power Generation

To validate the performance of the designed AST based harvester, lab tests were conducted under various flow rates with different resistive loads attached. The experimental setup is shown in Figure 5.3. A 5-ft schedule 40 PVC pipe with a diameter of 2 in (51 mm) was used to rebuild the water injection well structure in the lab environment. The flow in pipe was propelled by a centrifugal pump, which can theoretically achieve a maximum flow rate

Table 5.1: AST SPECIFICATIONS.

Symbol	Parameter	Value
D	Outer diameter	$50mm$
d	Inner diameter	$8mm$
N	Number of blades	2
D_p	Pipe diameter	$51mm$
L	Screw length	$85mm$
P	Screw pitch	$45mm$

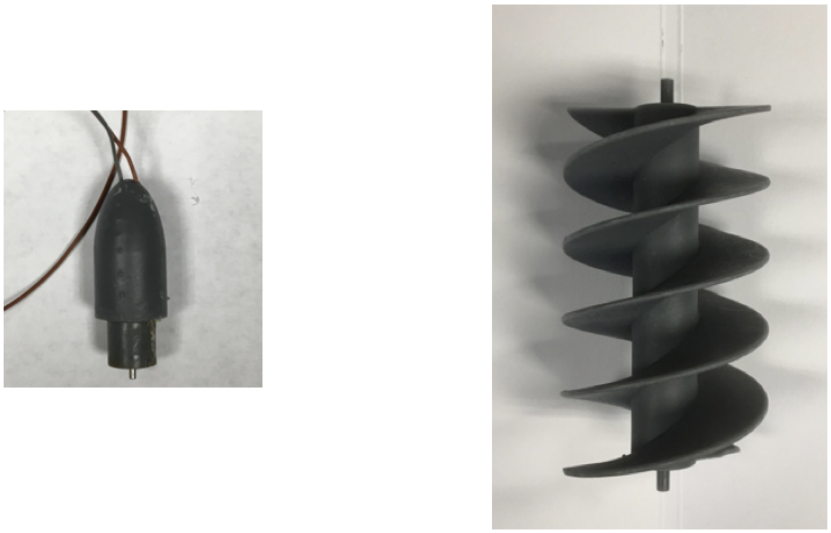

Figure 5.1: PRINTED GENERATOR CASING WITH GENERATOR INSIDE (LEFT) AND PRINTED AST (RIGHT).

of 20 GPM (1.26 L/s). To achieve the various flow rates needed for the test, a valve was attached to the outlet of the pump to adjust the flow. A flow meter with a flow range of 2 - 35 GPM $(0.13 - 2.21 L/s)$ and a 0.1% accuracy was used to measure the flow rate in the pipe. The AST based energy harvester was installed in the middle as a section of the pipe. In the experiments, 9 flow rates were tested, 0.44 L/s, 0.50 L/s, 0.57 L/s, 0.63 L/s, 0.69 L/s, 0.76 L/s, 0.82 L/s, 0.88 L/s, and 0.95 L/s. For each flow rate, 9 resistive loads were connected, 5 Ω, 10 Ω, 15 Ω, 20 Ω, 25 Ω, 30 Ω, 35 Ω, 40 Ω, and 45 Ω. The experimental results were measured using a DAQ system called CoCo-80 from Cristal Instruments. The generator used is a Commercial DC motor from Maxon. The specifications of the generator are listed in Table 5.2.

The experimental results were collected as the voltage reading across the resistive load over

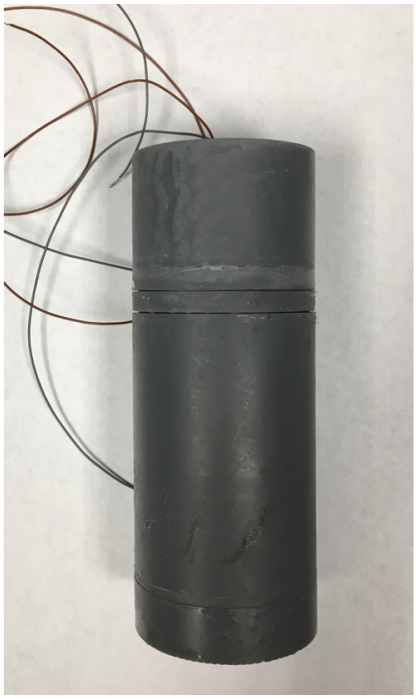

Figure 5.2: 3D PRINTED PROTOTYPE AFTER ASSEMBLY.

a period of 20 seconds and the average voltage was calculated. Experimental results are presented in Figure 5.4. The voltage was expected to increase quadratically as the flow rate increased. Due to the low-flow-rate nature of the setup, the voltage, in the lab test, appeared to have a linear relationship with the flow rate. The voltage across the resistive load kept increasing as the resistance increased until it reached 35 Ω; after 35 Ω, there seemed to be little change in the voltage reading. The maximum voltage recorded was 2.53 V, which occurred under a flow rate of 0.95 L/s and when a resistive load of 35 Ω was connected. However, this does not mean that 35 Ω is the optimal resistance, since the power is the result of both voltage and resistance; higher voltage with a higher resistance could result in a lower power output.

Then the average voltage output was converted to power output using the following equation, and presented in Figure 5.5.

$$Power = \frac{Voltage^2}{Resistance}$$

The power output appears to be quadratically related to the flow rate, which was expected because of the quadratic relationship between the voltage and power. The maximum power output was calculated to be 0.21 W, which occurred when the system was under a flow rate of 0.95 L/s and a resistive load of 10 Ω was connected.

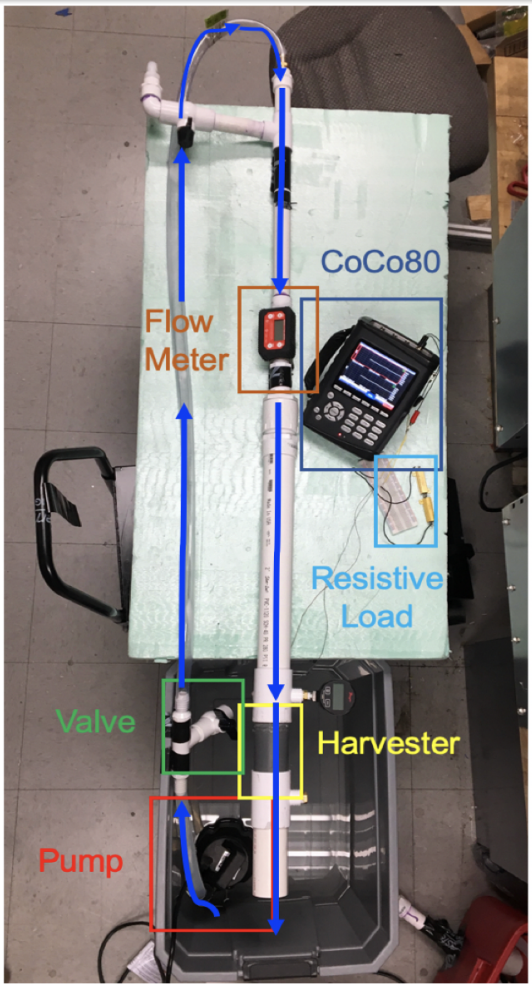

Figure 5.3: LAB TEST SETUP.

Because of the limited space inside the harvester and pipe environment, a torque meter and an encoder could not be installed. Thus, two important characteristics of the harvester, torque generation and rotational speed, could not be measured directly. As a result, such information can only be calculated using experimental data and the characteristics of the generator. The the operating speed can be calculated using the output voltage and speed constant of the generator.

$$V_g = \frac{V(R_l + R_m)}{R_l} = k_e \dot{\theta}_g$$

where V_g is the voltage across the generator, V is the voltage across the resistive load, R_l is the load resistance, R_m is the generator's terminal resistance, k_e is the speed constant of the generator, and $\dot{\theta}_g$ is the rotational speed of the generator.

Table 5.2: GENERATOR SPECIFICATIONS.

Symbol	Parameter	Value
R_m	Terminal resistance	2.58Ω
L_m	Terminal inductance	$0.008mH$
K_t	Torque constant	$7.79 \times 10^{-4} Nm/A$
K_e	Speed constant	$7.79 \times 10^{-4} Vs/rad$
I_m	Rotor inertia	$0.0166gcm^2$
I_g	Gear head inertia	$0.001gcm^2$
N_g	Gear ratio	57

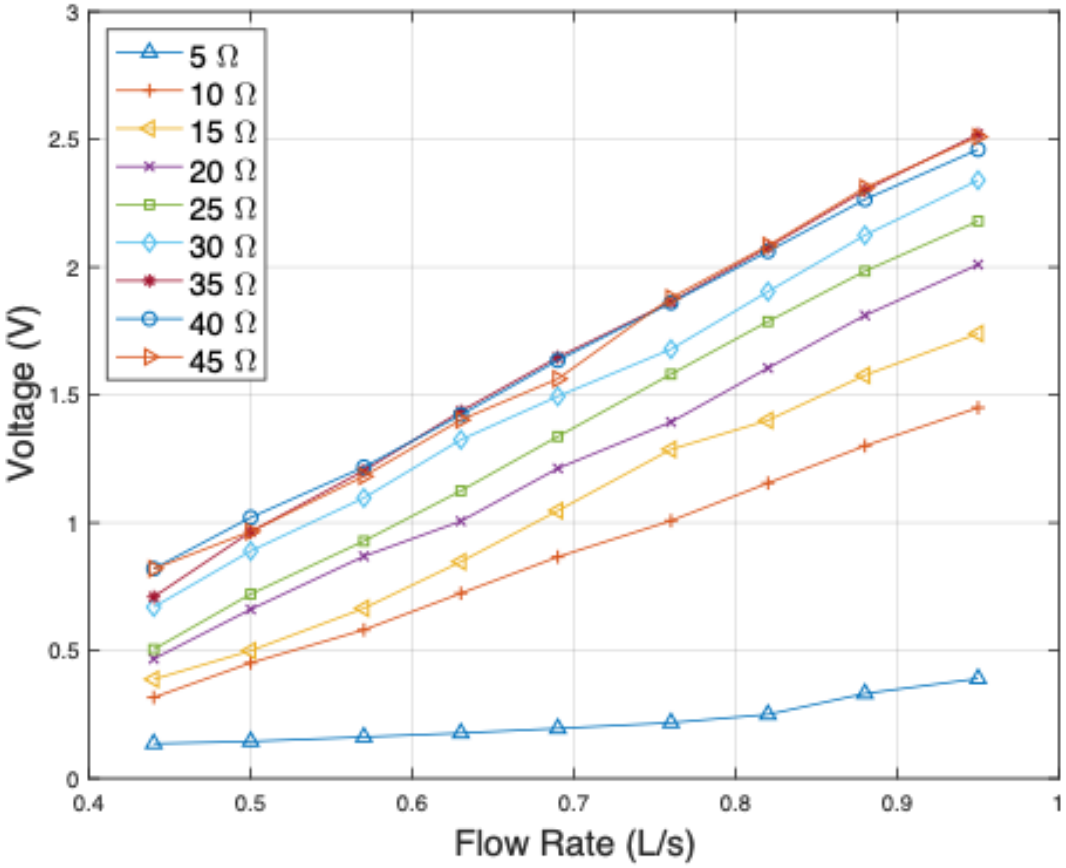

Figure 5.4: AVERAGE VOLTAGE VS FLOW RATE WITH DIFFERENT RESISTIVE LOADS.

The rotational speed of the AST can then be calculated using the generator's gear ratio N_g.

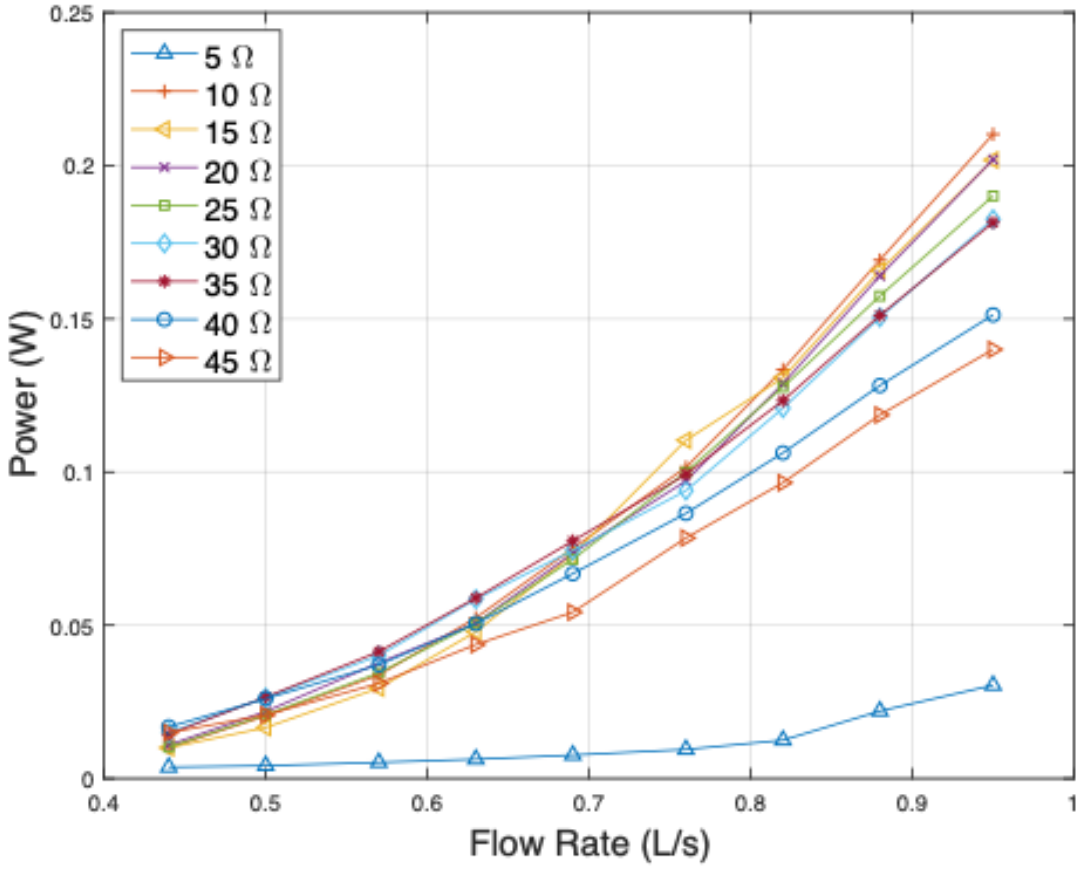

Figure 5.5: AVERAGE POWER VS FLOW RATE WITH DIFFERENT RESISTIVE LOADS.

$$\dot{\theta} = \frac{\dot{\theta_g}}{N_g}$$

The current generated in the circuit I can be calculated according to Kirchoff's voltage law.

$$k_e\dot{\theta_g} = IR_l + IR_m \Rightarrow I = \frac{k_e\dot{\theta_g}}{R_l + R_m}$$

The torque produced by the generator is related to the torque constant and generator current.

$$\tau_g = k_t I = \frac{k_e\dot{\theta_g}}{R_l + R_m}\dot{\theta_g}$$

The torque produced by the generator is linearly proportional to the rotational speed $\dot{\theta}$, hence the generator can be treated a s a damping term, where the electrical damping coefficient can be written as the following.

$$c_e = \frac{k_e \dot{\theta}_g}{R_l + R_m}$$

With the generator's terminal resistance being constant, the electrical damping c_e is a function of only the resistive load R_l. The relationship between the electrical damping c_e and the resistive load R_l is depicted in Figure 5.6

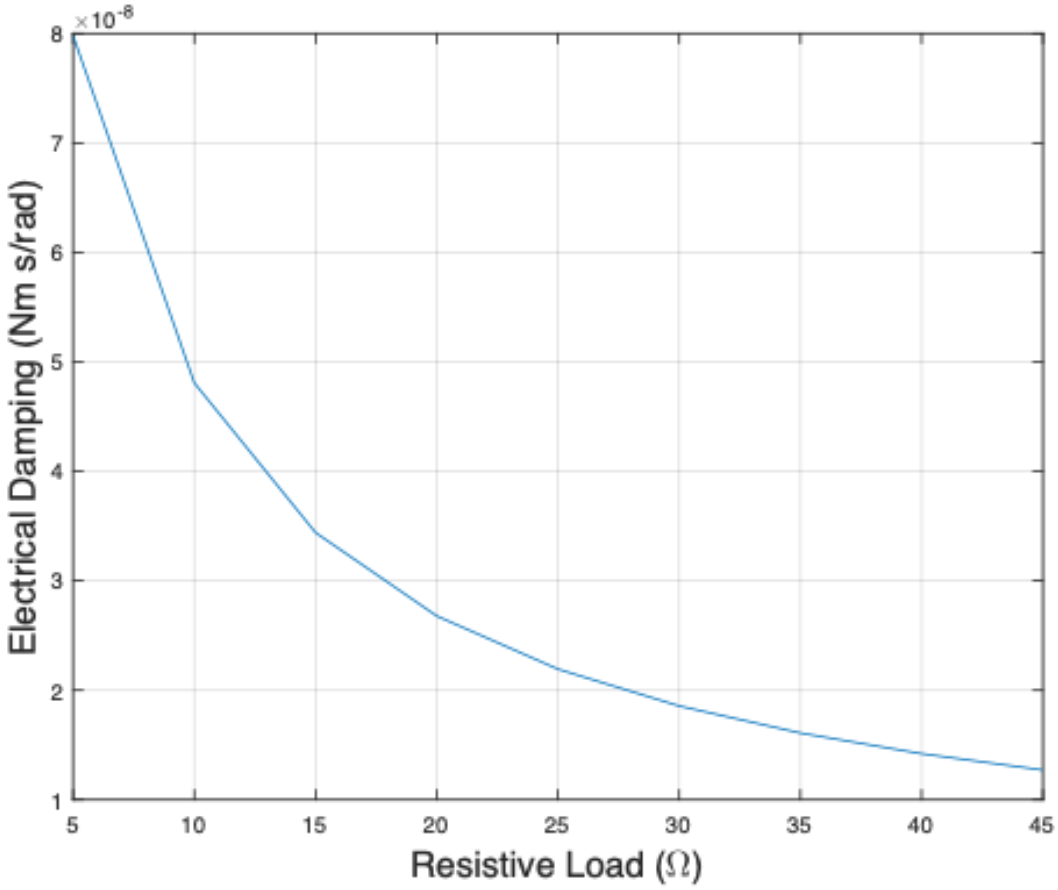

Figure 5.6: EQUIVELENT ELECTRICAL DAMPING VS RESISTIVE LOAD.

The expected power output from the CFD simulation can be expressed as the following.

$$P_{CFD} = (\tau_{CFD} - \tau_f - c_m \dot{\theta})\dot{\theta}$$

τ_f is the torque resulted from friction in the system whose value is unknown but constant. It is only dependent on the rotational direction but not the speed. c_m is the mechanical damping, whose value is also not known. Both the friction torque τ_f and the mechanical damping c_m could not be obtained directly.

Figure 5.7 shows the comparison between the numerical simulation and the experimental result when a resistive load of 10 Ω is connected.The difference between the simulation and experiments is the results of frictional torque and mechanical damping in the system, as the simulation did not take these two into consideration. The power loss due to mechanical damping is proportional to the rotational velocity of the AST, which explains the increased difference between the simulation and the experiments at higher RPM range.

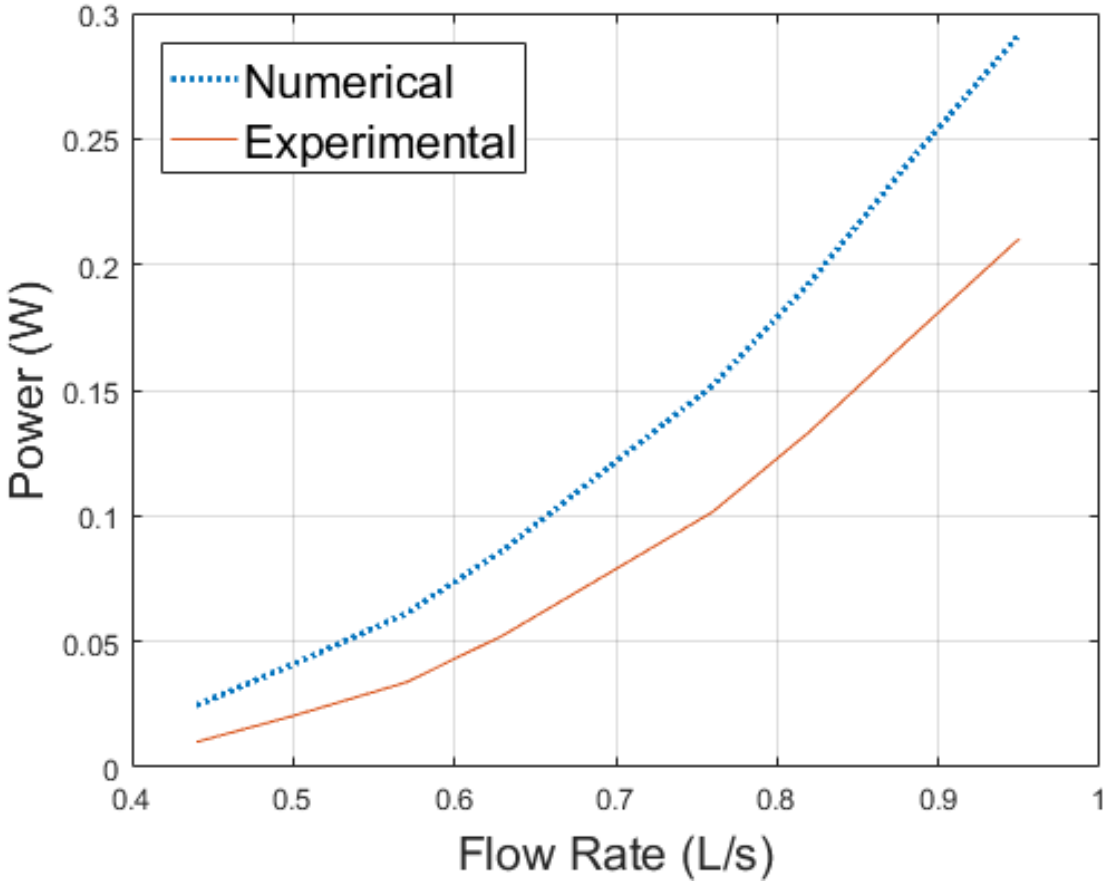

Figure 5.7: NUMERICAL SIMULATION AND EXPERIMENTAL RESULTS OF TORQUE AND POWER PRODUCED BY GENERATOR (LOAD = 10 Ω).

Table 5.3: SAM-1 UNDERWATER ACOUSTIC MODEM SPECIFICATIONS.

Property	Parameter
Size	135 mmL * 40 mmD
Weight	230 g
Depth Rating	300 m max
Operating Temperature	0 - 70 degree Celsius
Data I/O	RS-232 serial data link
Serial Buffer Size	32 *bytes*
TX Power	183 dB @ 8 V - 189 dB @ 16 V
Transmitting Frequency	Single channel 38.7 kHz
Data Rate	154 *bps*
Receiving Threshold	85 dB - 125 dB
Sonar Range	100 - 1000 m

5.2 Acoustic Communication

To test the acoustic communication in water filled-pipes, a pair of commercial underwater acoustic modems called SAM-1 from Desert Star were used. 17 PVC pipes with 5 cm in diameter and 3 m in length were used to form the pipeline system. The SAM-1 modem has a geometry of a cylinder and a geometric size of $135mmL * 40mmD$. The modem supports the RS-232 communication I/O standard, a single channel transmission frequency of 20 kHz. It requires a supply voltage of 8 V - 16 V to operate, which correspond to the transmitting intensity of 183 dB - 189 dB. The modem has a receiving threshold of 85 dB - 125 dB, which can be adjust to suit environments with different noise level. Any signal with a intensity lower than the threshold will not be picked up successfully by the receiving end of the modem. The SAM-1 underwater acoustic modem supports a data rate of 154 *bps*. The power consumption is relatively low, with a receiving power consumption of up to 0.168 W, and a peak transmitting power consumption of up to 32 W. The max rated distance of transmission is 1000 m in open water environment. The specifications of the used modem is summarized in Table 5.3.

Figure 5.9 shows a sample terminal window of the data transmission. ### command switches the modem into command mode, where transmitting speed, receiving frequency and threshold can be set using commands S, R, T respectively. A failed transmission is defined by either a missing character (lost) or a character that is not interpretable (shown as a # in the terminal). The performance of the transmission was characterized by $CER(CharacterErrorRate)$, which is equal to the percent of the unsuccessful transmission out of the total transmission performed.

Figure 5.8: DESERT STAR SAM-1 ACOUSTIC MODEMS

$$CER = \frac{\#of failedtransmission}{\#oftotaltransmission}$$

The modems were first tested in the open water between two piers to ensure the functionality of the modems. The distance between the two piers is around 80 m according to google maps.

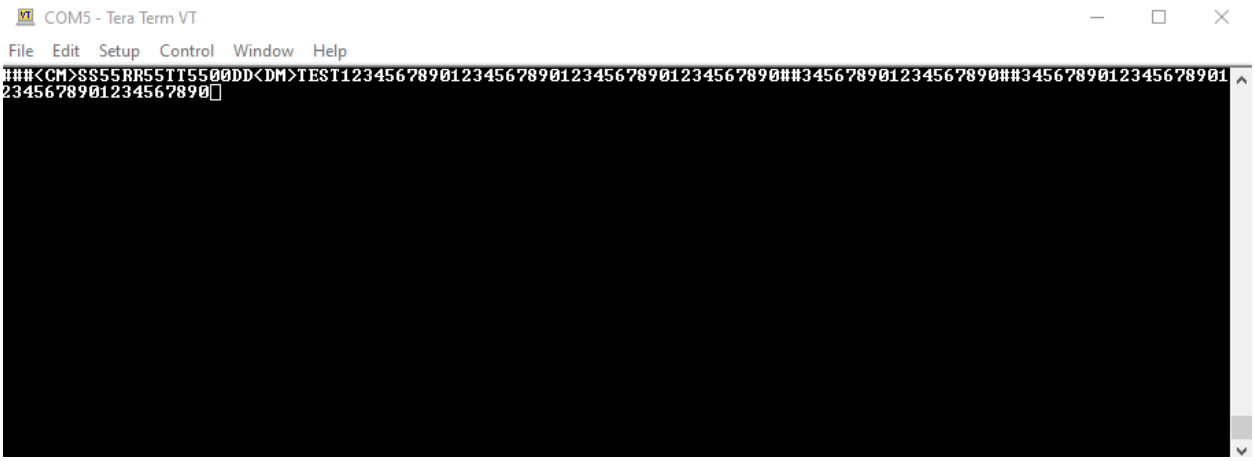

Figure 5.9: TERMINAL OF ACOUSTIC MODEM TRANSMISSION

The receiving threshold were varied in order to find out what intensity range works under this circumstance. Acoustic communication was successful even at the highest intensity threshold 183 dB, which implies that the attenuation of the acoustic signal attenuation is below 1dB/s. The receiving modem was able to pickup the communication signal as we kept lowing the receiving threshold until 109 dB. below this threshold, the transmission became unclear. This is due to the ambient noise in the lake. As the threshold was lowed to a certain level, the Signal to Noise ratio was lowered to a level so that the signal could not be recognized by the system.

Figure 5.10: OPEN WATER TEST WITH THE MODEMS. LEFT: IMAGE OF THE TEST SITE. RIGHT: GOOGLE MAPS SATELLITE VIEW.

To investigate the attenuation of the acoustic signal in the water-filled pipe, sections of pipes with a length of 3 m each were connected together to form a long pipeline. The acoustic modem pair are installed on the ends of the pipe, forming a closed system. Two computers are connected to the modem pair, one as the transmitting terminal, and the other one as the

Table 5.4: ACOUSTIC COMMUNICATION RESULT IN 6M PIPE WITH A RECEIVING THRESHOLD OF 125 DB

Total Transmission	Number of Success	CER
100	98	2%

receiving terminal. The modems were powered by a 8-V voltage source, which results in a signal intensity of 183 dB at the transmitting end. For each test setup, signal transmissions were performed by sending 100 characters through the pipe. Test was first conducted using a pipe with a length of 6 m with two PVC connected with a connector. Due to the limited space in the lab, the experiment was conducted in the open field at a backyard. The pipe was placed on the wooden floor of a balcony. The experimental set up is shown in Figure 5.11. The acoustic communication was able to pass through even with the highest threshold setting (125 dB).

The communication through pipe reached an almost 100% success rate. It is of crucial importance that once the harvester is installed in the pipe, it will not block the acoustic communication of the modems, so that they can form a truly wireless communication system for oil field applications. To test the compatibility of the designed harvester, the harvester is installed in the middle of a 6 m pipe (composed of 2 3-m pipes connecting together). The experimental set up is similar to the one to test acoustic modem performance without the harvester, with one SAM-1 modem installed on each end of the pipe. Two computers were used as terminals for data transmitting/receiving purposes. The pipe is filled with water. The experimental setup is shown in Figure 5.11. two sets of tests with the harvester running at different speeds were conducted to test the impact of the harvester of the in-pipe acoustic communication. Since only standing water was tested in the current phase, there would be not flowing water in the pipe to drive the harvester. Instead, the harvester was connected to a power supply with different voltages to drive the Archimedean Screw Turbine inside, to simulate the working condition of the harvester. The voltage supply was varied to generate different working RPM of the harvester. The first test was conducted with the harvester installed but not running; the Archimedean Screw Turbine stayed stationary through out the experiment. The second set of test was conducted with the harvester connected to a power supply of 1.5 V. The third test was conducted with the harvester connected to a power supply of 3 V. Each of the tests were repeated with 100 transmission conducted for each set. In total 300 transmissions were conducted. The results are compared with transmission with no harvester integrated at the same distance. The installed harvester does not appear to have significant impact on the transmission success rate. For a more rigorous test, a pair of hydrophones are needed to measure the exact pressures at both the transmitting end and receiving end to determine the attenuation and the impact of the harvester on the acoustic communication. The results are shown in Table 5.7

Table 5.5: ACOUSTIC COMMUNICATION RESULT IN 6M PIPE WITH HARVESTER INTEGRATED

Applied Voltage	Total Transmission	Number of Success	CER
0 V	100	98	2%
1.5 V	100	94	6%
3 V	100	96	4%

Table 5.6: ACOUSTIC COMMUNICATION RESULT IN 2M PIPE WITHOUT INTEGRATED HARVESTER

Receiving Threshold	Total Transmission	Number of Success	CER
105 dB	300	286	5%
107 dB	300	46	85%

After the 6m test was done, acoustic communication was then done in a pipe with a length of 12 m. Three PVC pipes were connected to form a long pipe. The pipes were initially placed on the grass ground. However, the signal would not propagate even after 6 m. The tremendous difference between this and the 6m test on the balcony implies that the contacting media (wooden floor on balcony and grass ground in this setup) has huge impact on the acoustic communication performance. To minimize the influence of the ground, the pipe was then lifted and supported on chairs. Figure 5.12 shows the experimental setup. Three transmissions with 100 character each were performed. The success rate changes dramatically when the receiving threshold was changed from 105 dB to 107 dB, which implies that the signal intensity at the end of the 12m pipe is somewhere between 105 dB and 107 dB. With a source intensity of 183 dB, the attenuation is approximated to be 6.5 dB/m. Table 5.6 shows the result of the acoustic communication without harvester.

Harvester was then installed in the middle of the 12 m pipe similar to the 6 m case to test the impact of the harvester on the acoustic communication. The receiving threshold was kept at 105 dB. The harvester was run at three different speeds with different applied voltage. The results are shown in Table **??**. The harvester appears to have minimum to no impact on the acoustic communication.

Table 5.7: ACOUSTIC COMMUNICATION RESULT IN 6M PIPE WITH HARVESTER INTEGRATED

Applied Voltage	Total Transmission	Number of Success	CER
0 V	100	96	4%
1.5 V	100	94	6%
3 V	100	94	6%

Figure 5.11: EXPERIMENTAL SETUP OF ACOUSTIC COMMUNICATION WITH INTEGRATED HARVESTER

Chapter 6

Summary and Future Work

In this study, the design of an Archimedean Screw Turbine based energy harvester was presented. Parametric study through CFD using Ansys Fluent was conducted. The impact of the number of blades were first analyzed. More comprehensive parametric study was then performed on AST length and AST pitch to determine the optimal geometry and operating condition of the AST. The relationship between the power generation and AST geometry was uncovered. The relationship between the optimal rotational speed and AST pitch was revealed. A prototype was fabricated through 3D printing. Lab test was conducted under different flow rates and different resistive loads to determine the maximum power generation.An average power out put of 0.21 W was achieved under a constant flow rate of 0.5 m/s and an external resistive load of 10 Ohm. On the acoustic communication side, the acoustic wave propagation inside water-filled pipes was simulated through FEA using the ACOUSTIC AND STRUCTURE INTERACTION MODULE of $COMSOLMULTIPHYSICS$. The acoustic attenuation was studied and characterized. Experiments on acoustic communication inside PVC pipes of various lengths were conducted using a pair of underwater acoustic modems from Desert Start to determine the acoustic attenuation through the pipe. Experiments were also conducted with harvester installed in the middle of the pipe to investigate the impact of the integrated harvester on the acoustic communication capability.

There are several things that are not considered in this phase of study, and will be in the scope of future work. One of the most important aspects of such turbine based energy harvester in a harsh environment like oil field downhole is harvester's life cycle. How long it will function before maintenance is required determines how much cost it will induce. For such energy harvester to be viable replacement of traditional batteries requires it to perform at least as long as the life of a battery before it drains power completely. A detailed study needs to be carried out in order to determine the life cycle of the current design and the necessary design changes that need to be made in order to extend the service life of the harvester. The harvester also needs to be integrated into the acoustic communication network, which requires a power management system and a power storage system. The power storage will

primary consists of a rechargeable battery. Since the harvester will function under constant flow rate, the output voltage will mostly be constant. To charge the battery reliably, at least a DC-DC converter is required for the power management circuit.

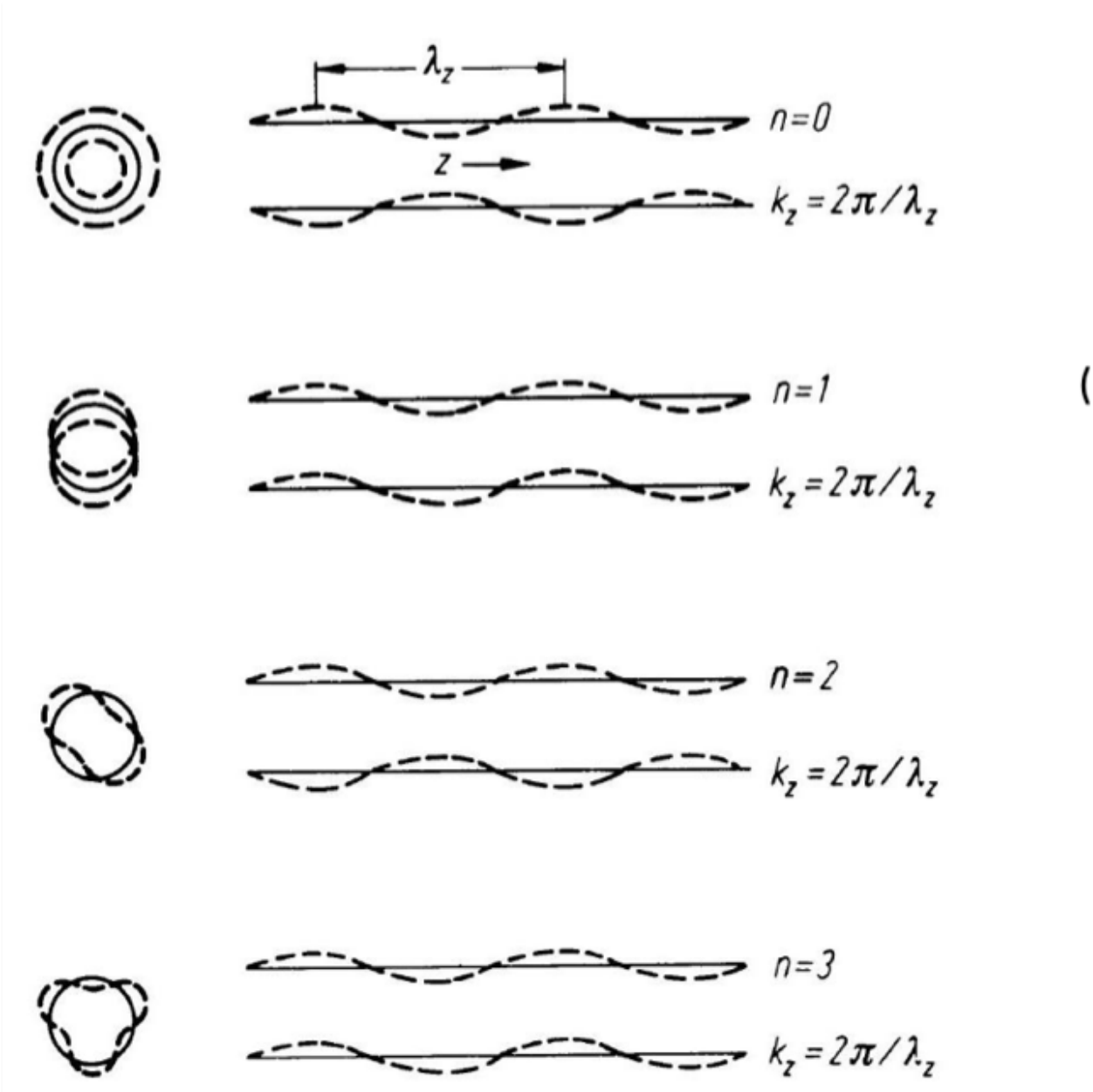

Figure 6.1: MODES OF WAVES IN A CYLINDRICAL PIPE

Another aspect that requires further study is the acoustic communication. In this study, the attenuation characteristics were investigated using a pair of underwater acoustic modems. The raw data of the acoustic wave intensity could not be extracted directly. As a result,

the attenuation characteristics were measured indirectly by changing the intensity threshold on the receiving end. The experimental results suggest an attenuation of 6 dB/m in the water-filled pipe, which is larger than expected and makes acoustic communication unsuitable for in-pipe applications. An attenuation this high could be the results of many factors such as wave frequency, pipe diameter, pipe wall thickness, pipe material, flow rate, obstacles in flow, the contacting media of the pipe, and etc. There have been other studies on acoustic wave propagation in liquid-filled pipes. However, most studies on acoustic wave and communication through the fluid media in pipe were focusing on lower frequency ranges (20 Hz 1000 Hz). Muggleton et al. (2003) conducted experiments on water-filled MDPE pipes buried in soil using frequencies ranging from 30 Hz to 1000 Hz. An attenuation of 10 dB/m was discovered under a wave frequency of 400 Hz. However, the frequency is too low compared to the kH range used for acoustic communication. The reason that many other studies done in this area were focused on low frequencies is because such frequencies were associated with leakage of the pipe and leakage detection was the focus of interest. For acoustic communication, most people invested the acoustic wave propagating through the pipe walls instead of the fluid media, which is not what this study is interested at. There have also been various works on the modeling of such systems and many have attributed the attenuation of acoustic wave in liquid-filled pipe to the acoustic and structural interaction between the liquid and the pipe wall (Moor et al, 2016). These studies suggest that below the ring frequency of the pipe, the n=1 and n=2 modes dominate. When the wave frequency exceeds the ring frequency, higher mods in the pipe wall will be induced. The ring frequency is the frequency at which of the wavelength of a longitudinal wave in the shell material equals its circumference, which is defined below.

$$\omega_r = \frac{c_l}{a}$$

$$c_l = \frac{E_s}{(\rho_s(1-v^2))(0.5)}$$

where c_l is the longitudinal wave speed in the shell plate, E_s is the Young's modulus of the material, v is Poisson's ratio, ρ_s is the density of the material, and a is the circumference of the pipe. The ring frequency of the pipe used in our study was calculated to be around 9 kHz. The wave frequency used in the acoustic communication was 32.8 kHz, which is a lot higher than the ring frequency of the PVC pipe. A study done by Fuller et al. in 1981 suggests that at higher frequencies, the acoustic energy will transfer between the fluid and the pipe structure, thus causing energy to dissipate into the surrounding environment contacting the pipe. This provides a potential explanation of the high attenuation experienced in the acoustic communication experiments.

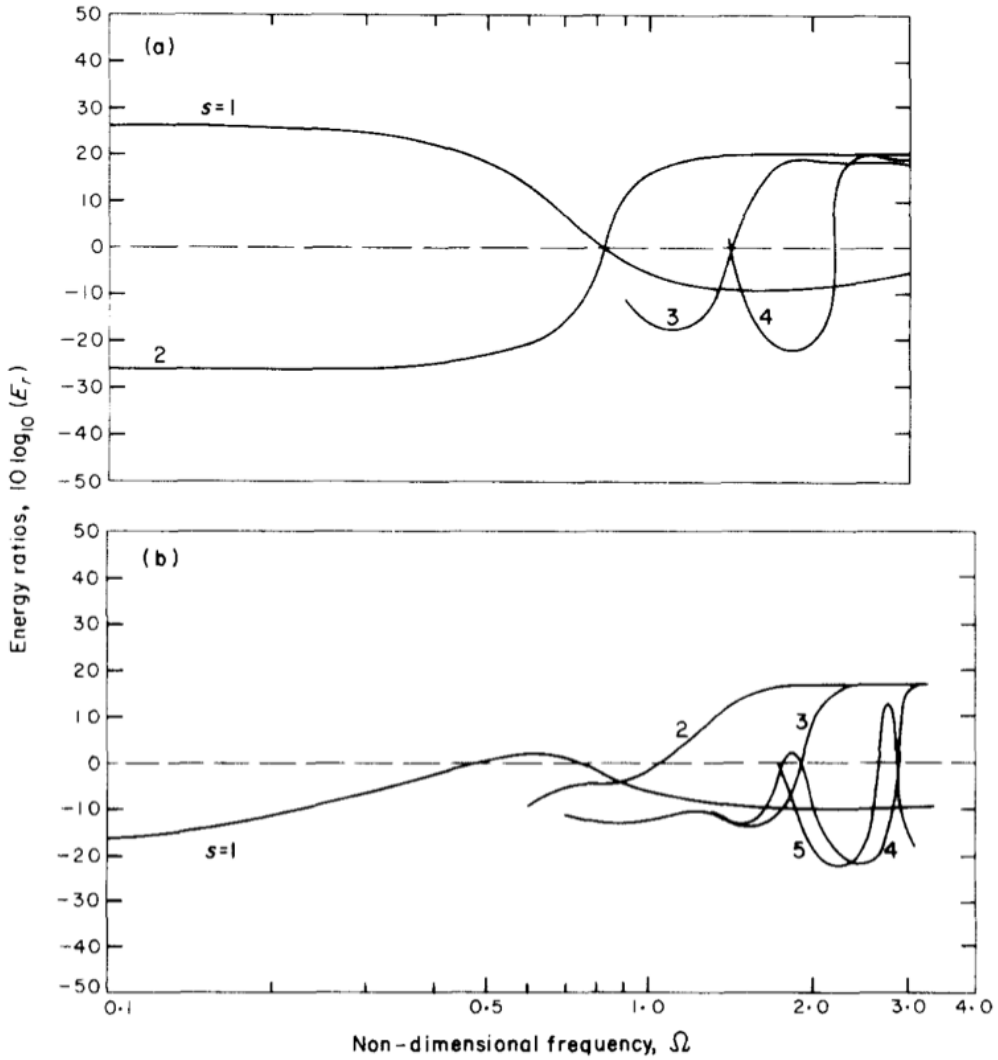

Figure 6.2: DISTRIBUTION OF VIBRATIONAL ENERGY IN A WATER-FILLED STEEL SHELL PIPE

Reference

Gungor, V.C. and Hancke, G.P. 2009. Industrial wireless sensor networks: Challenges, design principles, and technical approaches. IEEE Trans. Ind. Electron., vol. 56, no. 10, pp. 4258–4265.

Hou, L. and Bergmann, N.W. 2010. System requirements for industrial wireless sensor networks. in Proc. 15th IEEE ETFA, Spain, pp. 1-8.

ON World Inc. "Oil and Gas Wireless Sensor Networks – A Market Dynamics Report. "Reasearchandmarkets.com. (accessed February 18, 2019).

Akhondi, M.R. Talevski, A. Carlsen, S. Petersen, S. 2010. Applications of Wireless Sensor Networks in the Oil, Gas and Resources Industries. 24th IEEE International Conference on Advanced Information Networking and Applications, pp.941-948.

Ahmad, Talha J., Noui Mehidi, and Mohamed N. Noui. "Energy Harvesting Powered Wireless Monitoring and Control in Oil and Gas." In SPE Middle East Intelligent Energy Conference and Exhibition. Society of Petroleum Engineers, 2013.

Trimble, A. Zachary. "Downhole vibration sensing by vibration energy harvesting." PhD diss., Massachusetts Institute of Technology, 2007

Lee, Hyeong, Stewart Sherrit, Luis Tosi, Phillip Walkemeyer, and Tim Colonius. "Piezoelectric energy harvesting in internal fluid flow." Sensors 15, no. 10 (2015): 26039-26062.

Ahmad, Talha J., Muhammad Arsalan, Michael J. Black, and Mohamed N. Noui-Mehidi. "Piezoelectric Based Flow Power Harvesting for Downhole Environment." In SPE Middle East Intelligent Oil and Gas Conference and Exhibition. Society of Petroleum Engineers, 2015.

G. Park, T. Rosing, M. D. Todd, C. R. Farrar, and W. Hodgkiss, "Energy Harvesting for Structural Health Monitoring Sensor Networks," Journal of Infrastructure Systems, vol. 14, no. 1, pp. 64-79, 2008.

L. Mateu and F. Moll, "Review of Energy Harvesting Techniques and Applications for Microelectronics (Keynote Address)," Microtechnologies for the New Millennium 2005, International Society for Optics and Photonics, pp. 359-373, 2005.

Ujihara, M., Carman, G. P., and Lee, D. G. (2007). Thermal energy harvesting device using ferromagnetic materials. Applied physics letters, 91(9), 093508.

J. Vazquez, M. A. Sanz-Bobi, R. Palacios, and A. Arenas, "State of the Art of Thermoelectric Generators Based on Heat Recovered from the Exhaust Gases of Automobiles," Proceedings of the 7th European Workshop on Thermoelectrics, no. 17, 2002.

E. E. Lawreence and G. J. Snyder, "A Study of Heat Sink Performance in Air and Soil for Use in a Thermoelectric Energy Harvesting Device," Proceedings of the 21st International Conference on Thermoelectronics, pp. 446-449, 2002.

D. C. Hoang, Y. K. Tan, H. B. Chng, and S. K. Panda, "Thermal Energy Harvesting from Human Warmth for Wireless Body Area Network in Medical Healthcare System," International Conference on Power Electronics and Drive Systems, PEDS 2009. International Society for Optics and Photonics, pp. 1277-1282, 2009.

S. Chalasani and J. M. Conrad, "A Survey of Energy Harvesting Sources for Embedded Systems," IEEE Southeastcon 2008, International Society for Optics and Photonics, pp. 442-447, 2008.

Li, Z., Zuo, L., Luhrs, G., Lin, L., & Qin, Y. X. (2012). Electromagnetic energy-harvesting shock absorbers: design, modeling, and road tests. IEEE Transactions on vehicular technology, 62(3), 1065-1074.

Liu, M., Lin, R., Zhou, S., Yu, Y., Ishida, A., McGrath, M., ... & Zuo, L. (2018). Design, simulation and experiment of a novel high efficiency energy harvesting paver. Applied energy, 212, 966-975.

A. H. Meitzler, H. F. Tiersten, A. W. Warner, and D. Berlincourt, "IEEE Standard on Piezoelectricity," New York: Institute of Electrical and Electronics Engineers, 1988.

Blevins, R.D., 1990. Flow-Induced Vibration, Van Nostrand Reinhold.

Sinha, J.K., Rao, A.R. and Sinha, R.K. 2005. Prediction of Flow-Induced Excitation in a Pipe Conveying Fluid. Nuclear Engineering and Design 235, 627-636.

Sinha, D.N., 2005. Power Generation in Pipeline: Report. Los Alamos National Laboratory, Report No. LA-UR-05-6354.

Pittard, M.T., Evans, R.P., Maynes, R.D. and Blotter, J.D., 2004. Experimental and Numerical Investigation of Turbulent Flow Induced Pipe Vibration in Fully Developed Flow. Review of Scientific Instruments 75 (7), 2393-2401.

Waters, Shaun, and George A. Aggidis. "Over 2000 years in review: revival of the archimedes screw from pump to turbine." Renewable and Sustainable Energy Reviews 51 (2015): 497-505.

Williamson, S. J., B. H. Stark, and J. D. Booker. "Low head pico hydro turbine selection using a multi-criteria analysis." Renewable Energy 61 (2014): 43-50.

Kibel, P. "Fish monitoring and live trials. Archimedes screw turbine, River Dart. Phase I Report: Live fish trials, smolts, leading edge assessment, disorientation study, outflow monitoring." (2007).

Okot, D. K. (2013). Review of small hydropower technology. Renewable and Sustainable Energy Reviews, 26, 515-520.

E. Niell, A. Erturk, Advances in Energy Harvesting Methods, New York: Springer, 2013.

J. Sirohi and R. Mahadik, "Piezoelectric Wind Energy Harvester for Low-Power Sensors," Journal of Intelligent Material Systems and Structures, pp. 1-14, 2011.

S. Pobering and N. Schwesinger, "A Novel Hydropower Harvesting Device," 2004 International Conference on MEMS, NANO and Smart Systems, ICMENS 2004 Proceedings, International Society for Optics and Photonics, pp. 480-485, 2004.

H. D. Akaydın, N. Elvin, and Y. Andreopoulos, "Wake of a Cylinder: A Paradigm for Energy Harvesting with Piezoelectric Materials," Experiments in Fluids, vol. 49, no. 1, pp. 291-304, 2010.

S. Shi, T. H. New, and Y. Liu, "Flapping Dynamics of a Low Aspect-Ratio Energy-Harvesting Membrane Immersed in a Square Cylinder Wake," Experimental Thermal and Fluid Science, vol. 46, pp. 151-161, 2013.

Taylor, G.W. Burns, J. R. Kammann, S.M., et al. 2001. The energy harvesting eel: A small subsurface ocean/river power generator. IEEE J. Ocean. Eng., vol. 26, no. 4, pp. 539-547.

Li, S. and Lipson, H. 2009. Vertical-stalk flapping-leaf generator for wind energy harvesting. in Proc. ASME Conf. Smart Mater., Adaptive Struct. Intell. Syst., pp. 611-619.

Schultz, R. L., Ringgenberg, P. D., Robison, C. E., Michael, R. K., & Bayh III, R. I. (2003). U.S. Patent No. 6,504,258. Washington, DC: U.S. Patent and Trademark Office.

Chen, K. C., Pabon, J. A., Ganguly, P., Ocalan, M., Guerrero, J. C., & Forbes, K. J. (2009). U.S. Patent No. 7,560,856. Washington, DC: U.S. Patent and Trademark Office.

Tosi, L. P. (2014). U.S. Patent No. 8,624,419. Washington, DC: U.S. Patent and Trademark Office.

Tips, T. R. (2007). U.S. Patent No. 7,242,103. Washington, DC: U.S. Patent and Trademark Office.

Tubel, P., Holcombe, M. W., Baugh, J. L., Mullins, I. A. A., & Ross, R. C. (1998). U.S. Patent No. 5,839,508. Washington, DC: U.S. Patent and Trademark Office.

Tinnen, B. M., & Sørtveit, H. (2014). U.S. Patent No. 8,786,113. Washington, DC: U.S. Patent and Trademark Office.

Marya, M. P., & Rytlewski, G. L. (2014). U.S. Patent No. 8,916,983. Washington, DC: U.S. Patent and Trademark Office.

Schultz, R. L., Fripp, M. L., & Watson, B. W. (2005). U.S. Patent No. 6,848,503. Washington, DC: U.S. Patent and Trademark Office.

Cousins, E. T. (2006). U.S. Patent No. 7,002,261. Washington, DC: U.S. Patent and Trademark Office.

Schoonover, L. G. (2013). U.S. Patent No. 8,581,427. Washington, DC: U.S. Patent and Trademark Office.

Hall, D. R., Dahlgren, S., Marshall, J., & Wilde, T. J. (2009). U.S. Patent No. 7,537,051. Washington, DC: U.S. Patent and Trademark Office.

Maurer, W., & McDonald, W. (2005). U.S. Patent Application No. 11/024,285.

Hall, D. R., Dahlgren, S., & Comfoltey, M. (2011). U.S. Patent No. 8,033,328. Washington, DC: U.S. Patent and Trademark Office.

Hardin Jr, J. R., & Sitka, M. (2013). U.S. Patent No. 8,604,632. Washington, DC: U.S. Patent and Trademark Office.

Akyildiz, I. F., Pompili, D., & Melodia, T. (2005). Underwater acoustic sensor networks: research challenges. Ad hoc networks, 3(3), 257-279.

AUV Laboratory at MIT Sea Grant, Available from ¡http://auvlab.mit.edu/¿.

X. Yang, K.G. Ong, W.R. Dreschel, K. Zeng, C.S. Mungle, C.A. Grimes, Design of a wireless sensor network for long-term, in-situ monitoring of an aqueous environ- ment, Sensors 2 (2002) 455–472.

B. Zhang, G.S. Sukhatme, A.A. Requicha, Adaptive sampling for marine microorganism monitoring, in: IEEE/RSJ International Conference on Intelligent Robots and Systems, 2004.

N.N. Soreide, C.E. Woody, S.M. Holt, Overview of ocean based buoys and drifters: Present applications and future needs, in: 16th International Conference on Interactive Information and Processing Systems (IIPS) for Meteorol- ogy, Oceanography, and Hydrology, January 2004.

E. Cayirci, H. Tezcan, Y. Dogan, V. Coskun, Wireless sensor networks for underwater surveillance systems, Ad Hoc Networks, in press; doi:10.1016/j.adhoc.2004.10.008.

Sendra, S., Lloret, J., Jimenez, J. M., & Parra, L. (2015). Underwater acoustic modems. IEEE Sensors Journal, 16(11), 4063-4071.

A. Sanchez, S. Blanc, P. Yuste, and J. J. Serrano, "A low cost and high efficient acoustic modem for underwater sensor networks," in Proc. IEEE-Spain OCEANS, Santander, Spain, Jun. 2011, pp. 1–10.

Long, R., Lowe, M., & Cawley, P. (2003). Attenuation characteristics of the fundamental modes that propagate in buried iron water pipes. Ultrasonics, 41(7), 509-519.

Baik, K., Jiang, J., & Leighton, T. G. (2010). Acoustic attenuation, phase and group velocities in liquid-filled pipes: Theory, experiment, and examples of water and mercury. The Journal of the Acoustical Society of America, 128(5), 2610-2624.

Graf, T., Gisler, T., Sollberger, P., & Schälli, O. (2014). Acoustic wave propagation in water filled buried polyethylene pipes. In Comsol Conference, Cambridge (Vol. 7, No. 2).

Pierce, A. D. Basic Linear Acoustics, Chapter 3 in Springer Handbook of Acoustics, Ed. TD Rossing.

Williamson, S. J., Stark, B. H., & Booker, J. D. (2014). Low head pico hydro turbine selection using a multi-criteria analysis. Renewable Energy, 61, 43-50.

Lubitz, W. D., Lyons, M., & Simmons, S. (2014). Performance model of Archimedes screw hydro turbines with variable fill level. Journal of hydraulic engineering, 140(10), 04014050.

Fiardi, E. (2014). Preliminary design of Archimedean screw turbine prototype for remote area power supply. Journal of Ocean, Mechanical and Aerospace-Science and Engineering, 5.

Lashofer, A., Hawle, W., & Pelikan, B. (2012, October). State of technology and design guidelines for the Archimedes screw turbine. In meeting of Hydro.

McNabb, C. D., Liston, C. R., & Borthwick, S. M. (2003). Passage of juvenile Chinook salmon and other fish species through Archimedes lifts and a Hidrostal pump at Red Bluff, California. Transactions of the American Fisheries Society, 132(2), 326-334.

Kibel, P. (Fishtek-C. L. . (2007). FISHTEK consulting Fish Monitoring and Live Fish Trials . Archimedes Screw Turbine , River Dart Client : Project :, 1–40.